THESIS FOR THE DEGREE OF DOCTOR OF PHILOSOPHY

On modelling of slope stability in sensitive clay

The effect of time and state

CAROLINA SELLIN

Department of Architecture and Civil Engineering

Division of Geology and Geotechnics

CHALMERS UNIVERSITY OF TECHNOLOGY

Gothenburg, Sweden 2023

On modelling of slope stability in sensitive clay
The effect of time and state
CAROLINA SELLIN
ISBN 978-91-7905-906-4

Department of Architecture and Civil Engineering
Division of Geology and Geotechnics
Chalmers University of Technology
SE-412 96 Gothenburg
Sweden
Telephone: +46 (0)31-772 1000

Cover:
Landslide scars at Smådala, Lilla Edet municipality, Sweden, in 1979 or earlier.
Photo: Åke Hillefors / Göteborgs naturhistoriska museum

On modelling of slope stability in sensitive clay
The effect of time and state
Thesis for the degree of Doctor of Philosophy
CAROLINA SELLIN
Department of Architecture and Civil Engineering
Division of Geology and Geotechnics
Chalmers University of Technology

ABSTRACT

The stability of natural slopes is a global problem, with the number of landslides and the associated socioeconomic losses increasing, as a result of the global trend of urbanisation, deforestation and changed weather patterns. The available methods for identifying potential failure modes and assessing the stability, however, overly simplify the modelled soil behaviour within a slope, which might lead to unnecessary mitigation measures or non-conservative results. On the other hand, advanced soil models suitable to capture the response of sensitive clays, have successfully been demonstrated for Serviceability Limit State problems in geotechnics. Yet, those advanced models have not been exploited for effective stress based slope stability analyses.

The aim of this thesis, therefore, is to explore and integrate advanced soil models for analysing the stability of slopes in natural sensitive clay. As such, the evolving hydromechanical processes known to be occurring in a slope, ranging from anisotropy to rate dependency, should be accounted for. The main research effort has consisted of; (i) verification of the use of an anisotropic failure criterion, based on the NGI-ADP model, in the upper bound limit analysis Discontinuity Layout Optimisation (DLO), and (ii) investigation the applicability of the advanced, rate-dependent, Creep-SCLAY1S model for analysing slope stability.

The result findings indicate that DLO is a most satisfactory alternative to the use of the NGI-ADP model in a Finite Element code, and a more robust alternative than Limit Equilibrium Method. Furthermore, the second part of the study showed that while it is feasible to use a rate-dependent model for slopes, great care needs to be taken to the initialisation of the state variables, most notably the effective stress state in the sloping ground. The best results were obtained by approximately simulating the geological formation processes leading to a natural slope. The gravity increase method, instead of the strength reduction method, was required to quantify the slope stability. Consequently, the rate of increasing the gravity, i.e. the rate of loading, was shown to have a significant impact on the mobilised shear strength, thereby also the calculated stability. Overall, this thesis has contributed to the understanding of the transient coupled hydromechanical processes acting in a natural slope, and have shown that simplifications are necessary for practical applications.

Keywords: slope stability, sensitive clay, anisotropy, mobilisation of shear strength, rate dependence, destructuration, constitutive modelling

ACKNOWLEDGEMENTS

So many people have joined, supported and helped me throughout this journey, words cannot express my gratitude to all of you and the page cannot fit all your names.

The senior staff at the Geotechnics Research Group and beyond; supervisors Minna Karstunen, Ayman Abed and Mats Karlsson, examiner Jelke Dijkstra, thank you all for your guidance, encouragement and for always taking your time for a discussion. My fellow doctoral students and accompanying postdocs; continue to be who and how you are.

I will always remember the time spent with you, including everything from sharing office with day-to-day weather observations to celebrations of progress and unwavering support through struggles. I am genuinely inspired by your kindness, curiosity and eagerness to learn more.

Finally, I would like to thank my family and friends for your unconditional love and support, in person and remotely. I am so lucky to have you in my life. Sebastian, thank you for your tremendous patience and understanding. Julia, thank you for keeping me grounded.

Carolina Sellin
Göteborg, 2023

LIST OF PUBLICATIONS

This thesis consists of an extended summary and the following appended papers:

Paper A   Sellin, C. (2019). On evaluating slope stability in sensitive clay -a comparison of methods through a case study. In D. Ülgen, A. Saygili, M. R. Kahyaoğlu, S. Durmaz, O. Toygar, & A. Göçügenci (Eds.), *Proceedings of the 27th European Young Geotechnical Engineers Conference* (pp. 249–254). Turkish Society for ISSMGE

Paper B   Sellin, C., Abed, A., Dijkstra, J., Karlsson, M., & Smith, C. C. (2023a). Anisotropic strength in discontinuity layout optimisation for undrained slope stability analysis. *Unpublished manuscript*

Paper C   Sellin, C., Karlsson, M., & Karstunen, M. (2023b). Impact of rate-dependency on slope stability in sensitive clays. *Manuscript submitted for publication*

Paper D   Sellin, C., & Karstunen, M. (2023). Slope stability assessment in sensitive clay with an advanced constitutive model. L. Zdravković, S. Kontoe, D. Taborda, & A. Tsiampousi (Eds.), *Proceedings of the 10th European Conference on Numerical Methods in Geotechnical Engineering* (pp. 1–6). CRC Press

The author has carried the main responsibility for the computational work presented in the appended papers, including methodology, visualisation and writing of original drafts. Co-authors have contributed with conceptualisation, supervision, reviewing and editing. Implementational work conducted for Paper B was carried out by Professor Colin Smith and co-workers at the University of Sheffield and LimitState Ltd.

OTHER RELATED PUBLICATIONS

◇ Karlsson, M., Sellin, C., & Karstunen, M. (2021). *Smådala slope : Evaluation of the stability of a natural slope with a creep model*. BIG (Branschsamverkan i Grunden). Göteborg, Sweden

◇ Palau, R. M., Capobianco, V., Gilbert, G. L., Solheim, A., Láng-Ritter, I., Perrels, A., Sellin, C., & Filla, S. (2022). Mitigation alternatives for natural hazards along Nordic infrastructure networks – early results from the NordicLink project. Þ. Saemundsson, Á. R. Hjartardóttir, B. Gautason, & H. Geirsson (Eds.), *The 35th Nordic Geological Winter Meeting 2022*. Sena ehf.

◇ Sellin, C. (2021). *A2017-10 Final Report : Effects of climate change on slopes in sensitive clay*. BIG (Branschsamverkan i Grunden). Göteborg, Sweden

TABLE OF CONTENTS

NOTATIONS

Other variables may appear.

Abbreviations

An	Anisotropy applied on active shear strength
APn	Anisotropy applied on active and passive shear strength
Pn	Anisotropy applied on passive shear strength
ADP	Active Direct Passive
BP	Before Present
CSL	Critical State Line
CSS	Current Stress State
DLO	Discontinuity Layout Optimization
DSS	Direct Simple Shear test
FCT	Fall Cone Test
FE	Finite Element
FELA	Finite Element Limit Analysis
FEM	Finite Element Method
ICS	Intrinsic Compression Surface
LEM	Limit Equilibrium Method
m.a.s.l	Meters above sea level
MCC	Modified Cam Clay
NCS	Normal Compression Surface
OCR	Overconsolidation ratio
OCR*	Generalized overconsolidation ratio
POP	Pre-overburden pressure
ULS	Ultimate Limit State
VST	Vane Shear Test

Greek symbols

α	Slope inclination
$\boldsymbol{\alpha}_d$	Deviatoric fabric tensor
α_0	Initial value of fabric anisotropy
α_{ij}	Fabric tensor component
$\alpha_{K_0^{nc}}$	Value of rotational anisotropy in normally consolidated state
β	Creep component in $\dot{\Lambda}$
γ	Shear strain
$\gamma^p_{(f)}$	Plastic shear strain (at failure)
γ^C_f	Shear strain at failure in triaxial compression
γ^{DSS}_f	Shear strain at failure in direct simple shear
γ^E_f	Shear strain at failure in triaxial extension
δ_{ij}	Kronecker delta
$\dot{\boldsymbol{\varepsilon}}$	Strain rate tensor; Total strain rate
$\dot{\boldsymbol{\varepsilon}}_d$	Deviatoric strain rate tensor
$\dot{\varepsilon}^{e,c}$	Elastic and creep strain rate, respectively
ε_a	Axial strain
$\dot{\varepsilon}_{ij}$	Strain rate component
$\dot{\varepsilon}_{v,d}$	Volumetric and deviatoric strain rate, respectively
η	Stress ratio, $p' : q$
$\eta_{K_0^{nc}}$	Stress ratio at normal consolidation
θ	Lode angle
θ_r	Principal stress direction
θ_α	Lode angle for the stress state on the α-line
κ	Volumetric hardening parameter in NGI-ADP

κ^*	Modified swelling index	F	Safety factor
$\dot{\Lambda}$	Viscoplastic multiplier	G'	Effective elastic shear modulus
λ^*	Modified compression index	$\hat{J}_2$	Modified second deviatoric invariant
λ_i^*	Modified intrinsic compression index	$(J_2)_\alpha$	Second invariant of the modified deviatoric stress
λ_{LEM}	Scaling factor of interslice resultant	$\hat{J}_3$	Modified third deviatoric invariant
μ^*	Modified creep index	$(J_3)_\alpha$	Third invariant of the modified deviatoric stress
μ_i^*	Modified intrinsic creep index		
v'	Poisson's ratio	K'	Effective elastic bulk modulus
ξ	Absolute rate of destructuration	K_0	Coefficient of earth pressure at rest
ξ_d	Relative rate of destructuration	K_0^{nc}	Coefficient of earth pressure at rest for normally consolidated soil
$\boldsymbol{\sigma}'$	Cartesian effective stress tensor		
$\boldsymbol{\sigma}'_d$	Deviatoric stress tensor	M	Stress ratio at critical state
σ'_{ij}	Effective stress component	M_c	Stress ratio at critical state in triaxial compression
σ'_{vc}	Vertical preconsolidation pressure		
σ_2	Intermediate total stress	M_e	Stress ratio at critical state in triaxial extension
$\sigma_{d,ij}$	Deviatoric stress component		
τ_{ij}	Shear stress component	$M(\theta)$	Stress ratio at critical state with Lode angle dependency
τ_{ref}	Reference time		
φ'	Critical state friction angle	m	Ratio $M_e : M_c$
χ	Amount of bonding	p'	Mean effective stress
$\dot{\chi}$	Destructuration increment	p'_{cs}	Mean effective stress at critical state
χ_0	Initial amount of bonding	p'_{eq}	Equivalent mean effective stress
ω	Shape function in NGI-ADP	p'_m	Isotropic preconsolidation pressure
ω	Absolute rate of rotational hardening	p'_{mi}	Intrinsic isotropic preconsolidation pressure
ω_d	Relative rate of rotational hardening	q	Deviatoric stress
Roman letters		q_{cs}	Deviatoric stress at critical state
		S_t	Sensitivity
a_1	Scale factor	s_u^A	Undrained active shear strength
c'	Cohesion intercept	$s_{u,inc}^A$	Change of undrained active shear strength with level
f	Yield criterion		

s_u^P Undrained passive shear strength ΣM_{stage} Gravity multiplier

s_u^{DSS} Undrained direct simple shear strength $\Sigma M_{gravity}$ Applied gravity

Miscellaneous ΣM_{weight} Target gravity

ΔF Relative change of safety factor $\langle\ \rangle$ Macaulay brackets

Part I
Extended summary

1 Introduction

1.1 Background

The stability of natural slopes has a significant impact on spatial planning and development, given the current global trend of urbanisation (United Nations and Affairs 2019) and changes in land use (Winkler et al. 2021). Furthermore, the impact extends to existing constructions and infrastructure that does not only have a risk of physical damage of assets (Guzzetti 2000; Li et al. 2021; Schlögl and Matulla 2018) but also severe societal consequences, including contaminated drinking water (Lundgren and Rapp 1974), loss of property value (Crosta et al. 2015) and negative effects on ecosystems (Geertsema et al. 2022).

The geotechnical problem of slope stability has been acknowledged for more than a century (Hultin 1916; Petterson 1916), with today's conventional methods for assessing the stability established over 50 years ago (Morgenstern and Price 1965; Spencer 1967). These traditionally used methods for soft soils include simplifications of the soil behaviour and force distribution, accordingly with a corresponding safety margin (Frank et al. 2015). However, as the climate is changing, so are also the changes in the hydromechanical conditions in the slope, potentially affecting the stability in unforeseen ways. This has perhaps already led to unnecessary mitigation measures or undetected risks for infrastructure or constructions.

Climate research has documented a global increase in the number of events of extreme temperatures and extreme precipitation respectively, and a further increase is projected in both intensity and frequency of extreme precipitation in Europe (IPCC 2021). Additionally, the mean temperature and the mean precipitation are projected to increase close to the poles, affecting northern Europe and northern North America in particular. As a consequence, rain-related flooding and erosion are estimated to increase, and it is estimated that one-third of the regions subjected to landslides today will have an increased number of landslides related to global warming (IPCC 2021; SGI 2022).

This calls for further exploration of the coupled hydromechanical processes, and the changes in the state of the soil within a slope. It will be increasingly important to consider transient mechanisms, accounting for both external factors, such as precipitation, as well as macro-mechanical and micro-mechanical changes. The latter two can be exhibited as erosion and rate-dependent soil structure, respectively. As summarised by Sowers and Sowers (1951):

> *In most cases a number of causes exist simultaneously, and so attempting to decide which one finally produced failure is not only difficult but also incorrect. Often the final factor is nothing more than a trigger that set in motion an earth mass that was already on the verge of failure. Calling the final factor the cause is like calling the match that lit the fuse that detonated the dynamite that destroyed the building the cause of the disaster.*

It is thereby essential to understand the current state of the soil in a natural slope before any future climate scenarios are added. In the context of numerical simulations of saturated soil, this requires the use of effective stress based analyses, preferably with advanced soil models that capture the soil behaviour in a changing environment. A first step, as will be the focus of this thesis, is to study the feasibility of using such models for slope stability analysis. For practical purposes though, these types of advanced slope stability assessments can only be applied to a limited number of geotechnical sites, while an initial screening is beneficial to detect such sites.

1.2 Aim and objectives

The overall aim of the project is to explore and integrate soil models for anisotropic, sensitive clay in slope stability assessment, to be able to account for evolving hydromechanical processes known to be occurring in a slope. The scope of the work has therefore been divided into five main objectives:

- Define and apply a benchmark case of a natural slope with existing excessive probing in sensitive clay (**Paper A, C, D**)

- Identify and compare a selection of available calculations methods for slope stability using an isotropic elastic/rigid-perfectly plastic soil model (**Paper A**)

- Investigate and verify the effect of an anisotropic total stress based soil model in a simplified numerical analysis (**Paper B**)

- Apply and evaluate the potential of an effective stress based, rate-dependent, soil model in slope stability assessment (**Paper C**)

- Numerically assess the effect of initial and strain-induced anisotropy and strain softening on the stability and failure mechanism in a slope (**Paper D**)

1.3 Limitations

- The soil type considered in this project is limited to soft sensitive clays, typical for the glacial and postglacial deposits in the Göta River valley, located southwest in Sweden. Similar geological history and soil properties can be found in other parts of Scandinavia, Russia and Northern America.

- Most field and laboratory investigations presented in the project were performed by external partners, sometimes in collaboration with Chalmers University of Technology, and were thus neither planned nor overseen by the author. No additional measurements were performed in the frame of this project, nor were any physical (full-scale or centrifuge) failure tests conducted.

- The comparative study of calculation methods is limited to four methods that were available in commercial software at the time the study started. Out of consistency, and accessibility in the software, all calculations in the comparative study were performed using Mohr-Coulomb as soil model.

- The effective stress based soil models used in the project are limited to the advanced rate-dependent Creep-SCLAY1S model, using its in-house implementation in the software PLAXIS 2D. Creep-SCLAY1S has previously shown good ability to capture the characteristics of soft sensitive clays (Amavasai et al. 2018; Hernvall et al. 2021; Tornborg et al. 2021), with a commercial version available via PLAXIS. The project does not consider any rate-independent precursors of the soil model.

2 On the characteristics of sensitive clays

The behaviour of an intact natural clay stems from its geological origin, including the orientation of particles and its chemical composition, and any subsequent micro- and macro-scale changes (Varnes 1958). Both geological processes and human activities (stress/strain history) affect the properties of the clay, ranging from its micro-structure and the apparent bonding between these particles, via the local conditions of a site with its topography, hydrogeology and stratification, to the geological scale with possible faults and plateaus. As discussed by Leroueil (2001), all these mechanisms interact to result in the observed behaviour in a slope, but this chapter focuses on the genesis and the observed behaviour on laboratory scale.

2.1 Geological origin and initial anisotropy

Soft sensitive clays, as most extensively found in Scandinavia and eastern Canada (Lefebvre 1996), originate from the sedimentation of fine-grained materials during and after the last glacial period. The weight of the local ice sheets, such as the Canadian Laurentide and the Scandinavian Fennoscandian (Kleman and Hättestrand 1999), pressed down the land surface and a significant amount of what today is land was below sea level.

In Scandinavia, the 2000-3000 m (Stroeven et al. 2016) thick ice sheet began to melt 22 000 years ago (Olsen et al. 2013), with grains of silt and clay depositing in the calm waters adjacent to the ice front. Areas below sea level continued to be submerged for a long period due to the slow process of the isostatic rebound, as shown in Figure 2.1. The isostatic rebound still continues today to various degrees, and locally counteracts the sea level rise (Nordman et al. 2023).
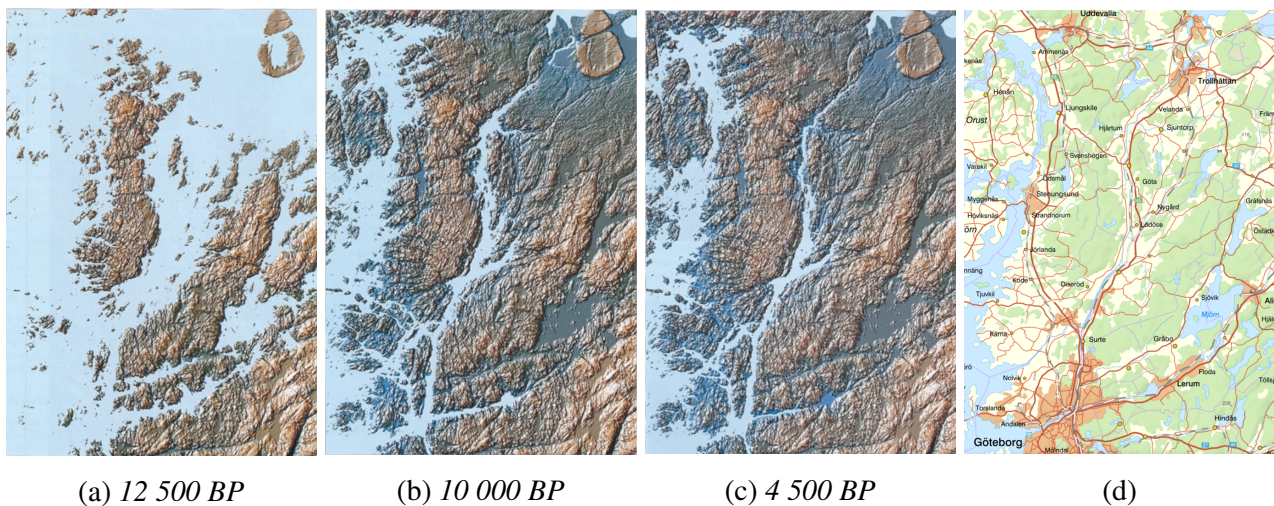

(a) *12 500 BP*   (b) *10 000 BP*   (c) *4 500 BP*   (d)

Figure 2.1: *(a-c) Palaeogeographical maps of the postglacial land uplift in the west of Sweden, given in years before present (BP). From Klingberg et al. (2006). (d) Current map of the same area, ©Lantmäteriet.*

As a result, the clay particles we encounter in the ground today have originally settled with a mainly horizontal orientation, and have subsequently experienced extensive dewatering due to self-weight consolidation, which is seen in a cross-anisotropic microstructure (Birmpilis et al. 2022; Burland 1990; Delage and Lefebvre 1984). These processes in combination with creep effects also explain the occurrence of apparent overconsolidation in soils that have never been unloaded. Naturally, the overconsolidation is further increased in valleys, originating from long-term erosion processes with expanding and meandering rivers.

2.2   Soil fabric and apparent bonding

The structure of a natural clay can be described as the combination of (i) the arrangement of particles and particle contacts, here called fabric, and (ii) the bonds acting between these particles (Quigley and Thompson 1966). The fabric orientation of intact clay and the bonding is the result of the geological deposition, where the bonding is not only governed by the ion concentrations during sedimentation but also by e.g. the presence of carbonates and organic matter (Leroueil and Vaughan 1990). A soft clay under loading behaves relatively stiff until yielding occurs, and the same clay under plastic straining demonstrates both a fabric rotation and softening behaviour. The former could lead to changes in the initial anisotropy, i.e. evolving anisotropy, while the softening behaviour is the result of the inter-particle bonds gradually degrading, referred to as destructuration (Leroueil et al. 1979). The presence of bonding in clay is also apparent when comparing the differences in peak strength envelope for overconsolidated clay to a non-bonded counterpart (Leroueil 2001; Leroueil et al. 1979). The destructuration results in a reduction in stiffness, which eventually leads to a completely remoulded/reconstituted clay.

One of the most extreme cases of destructuration is quick clay, where initial high ion concentrations have decreased due to natural leaching, such as rainwater infiltration, artesian pore pressures or diffusion (Rankka et al. 2004). The bonding in these quick clays can be instantaneously lost when subjected to any kind of disturbance, with some limited recovery associated with aging and thixotropy.

2.3   Rate-dependent behaviour

The rate-dependency observed in the stress-strain behaviour of soft clay originates from (i) the hydraulic properties and (ii) the arrangement of clay particles, and the importance of the two mechanisms depends on the applied strain rate and the stress history of the soil. At large strain rates and below the pre-consolidation pressure, the hydraulic conductivity governs the rate at which excess pore pressures can dissipate. Any apparent peak strength is thereby dependent on the strain rate, as shown by e.g. Casagrande and Wilson (1951), Graham et al. (1983a), Graham et al. (1983b), Lefebvre and LeBoeuf (1987), Sällfors (1975), Tavenas et al. (1978), Vaid et al. (1979), Yin et al. (2010), and Zhu et al. (1999). At lower strain rates, typically induced by a constant load or gravity, the re-arrangement of the clay particles (i.e. the fabric) is the governing mechanism, causing a tendency to creep (Birmpilis et al. 2022; Burland 1990), with a stress state over the preconsolidation.

The triaxial tests by Tavenas and Leroueil (1977) and Tavenas et al. (1978) suggest that the rate-dependency does not significantly change the initial anisotropy of the soil, although some fabric re-arrangement is expected, but rather affects the size of the yield surface, as seen in Figure 2.2, where each point represents a separate triaxial test on the same soil.
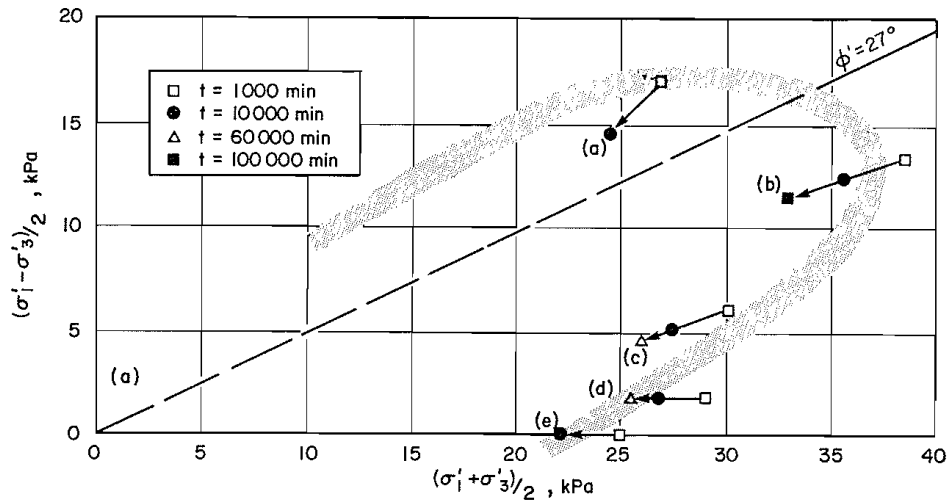

Figure 2.2: *Change of yield surface with load increment duration in triaxial tests. From Tavenas et al. (1978).*

In slope stability context, the rate-dependent behaviour of the soil in terms of pre-failure movements has different behavioural patterns depending on the cause of the instability. As pointed out by Emery (1978) and Terzaghi (1950), the movements can either be seasonal along an existing shear band (Comegna et al. 2013; Desai et al. 1995; Vulliet and Hutter 1988) or continuous in either parts of the slope or in the whole soil mass (Eden 1977; Saito 1965).

2.4 Mobilisation of strength

A slope failure is typically a progressive event (Take and Bolton 2011), with the mobilisation of the soil strength dependent on the historical and current stress state, and the corresponding changes in soil structure. The mobilised strength is therefore varying with the stress state within a slope, as illustrated in Figure 2.3. Here, the in-situ stress and chosen stress path clearly result in different locations of the yields points and thereby also the corresponding peak strengths.
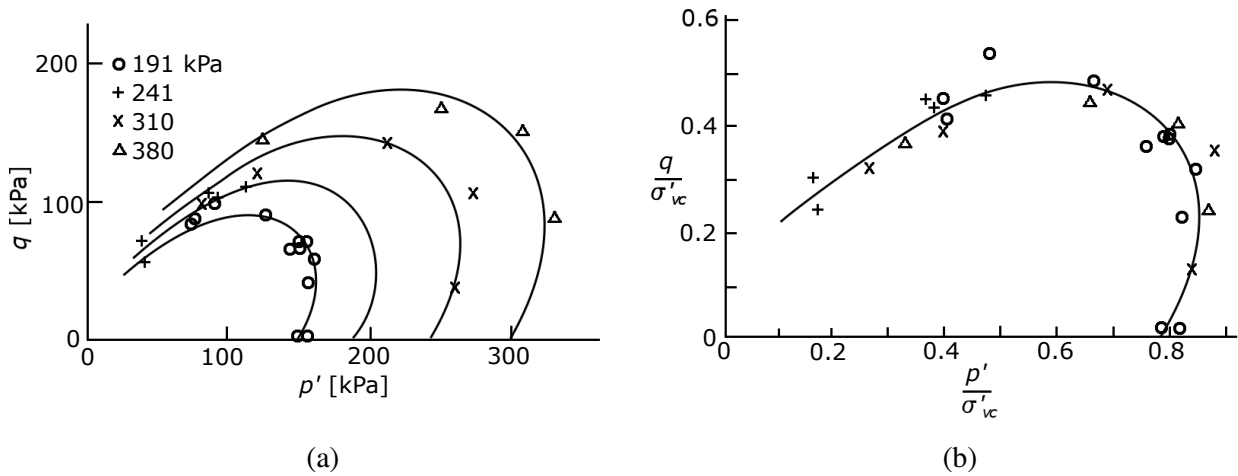
Figure 2.3: *Yield curves derived from triaxial tests performed on Winnipeg clay from four different depths. (a) Yield curves in mean effective stress-deviator stress ($p' - q$) space (b) yield curves normalised with preconsolidation pressure (σ'_{vc}). Adapted from Graham et al. (1983b).*

The effect of stress history and stress path is further illustrated in Figure 2.4, where simulations of undrained triaxial tests have been performed using an anisotropic model with stiffness degradation. This snapshot of the shape and orientation of the yield surface, shows how the vertical Overconsolidation Ratio (OCR) and the respective K_0 (coefficient of earth pressure at rest) affect not only the mobilised peak strength of the soil, but also the strain at the peak. The effective stress path is plotted in term of the mean effective stress-deviator stress ($p' - q$) space (a), axial strain ϵ_a vs deviator stress (b) and ϵ_a vs the stress ratio q/p' (c). As the effective stress path reaches the yield surface, excess pore pressures start to build up, and destruction of the inter-particle bonds accelerates until failure at the critical state is reached. The mobilised strength is thus a complex parameter with a major influence in slope stability assessment and care should be taken when simplifying the undrained strength to a single value.
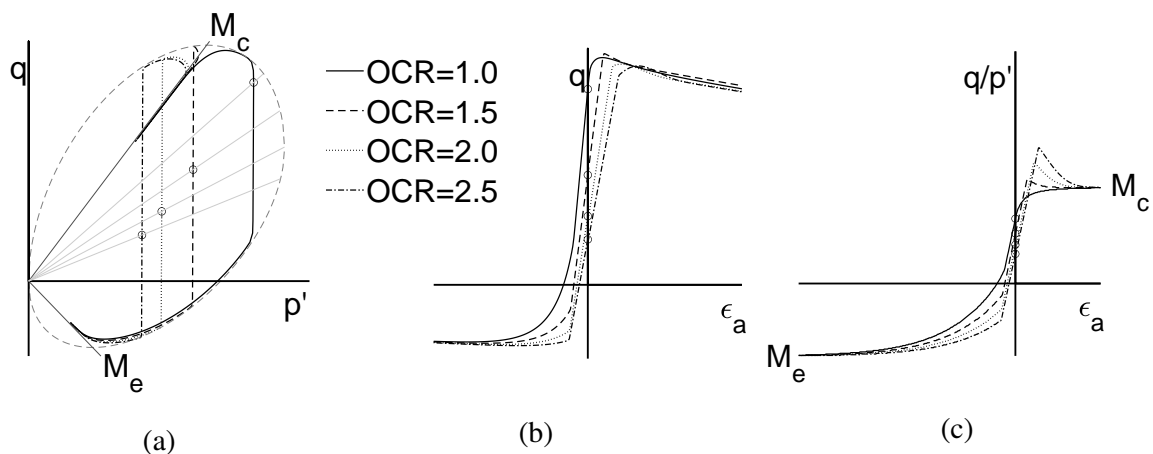

Figure 2.4: *Schematic presentation of triaxial tests in compression and extension with different OCR. M_c refers to the slope of the critical state line in compression and M_e is the corresponding slope for extension. From Paper C.*

9

3 Modelling of soft clays

Soil modelling, specifically for slope stability assessment, ranges from system-level physical tests in full-scale (Lafleur et al. 1988; Lehtonen 2011) or small-scale (Liang and Knappett 2017; Lucas et al. 2020), to element-level theoretical modelling (Davis and Christian 1971; Li et al. 2022). The latter is here limited to constitutive models, which create the mathematical framework to describe the generalised stress-strain response of the soil elements. The constitutive models are typically developed from observations at laboratory scale, and should ideally replicate the soil behaviour as found both on element- and system-level. However, once a constitutive model attempts to describe an increasingly complex soil behaviour, the mathematical framework expands, as further discussed in the following sub-chapters. Still today though, not all aspects of soil behaviour are fully understood and the constitutive model chosen should include sufficient features to simulate the type of soil response needed for the specific geotechnical problem.

One of the most accessible constitutive models is the Mohr-Coulomb model, which assumes a linear elastic-perfectly plastic behaviour and only accounts for the major and minor principal stress. When combined with (system-level) slope stability analyses using the conventional Limit Equilibrium Method, the soil behaviour is further reduced to a rigid-perfectly plastic response, i.e. only a failure criterion is considered. This allows for a fast and straightforward slope stability assessment but requires crude add-ons to account for the evolution of soil response observed in soft clays during plastic straining. For that case, the system-level modelling of an Ultimate Limit State is acceptable, but there is very little similarity to the observed element-level response.

The following sub-chapters will describe the additional two constitutive models used in the thesis; (i) the total stress based anisotropic NGI-ADP model and (ii) the advanced, rate-dependent, effective stress-based model Creep-SCLAY1S. The former uses an anisotropic modification of Tresca's failure criterion, which effectively circumvents the use of anisotropic add-ons in the Mohr-Coulomb model for total stress (undrained) analyses in slope stability assessment. The mathematical framework is still straightforward, with focus on system-level and justifiable simplifications on element-level. The latter one, Creep-SCLAY1S, is defined using the critical state concept, with the advantage of being applicable to several geotechnical scenarios, both on system- and element-level, and automatically accounts for hydromechanical response given it is an effective stress model, but with the drawback of e.g. many material parameters and a complex mathematical framework.

3.1 NGI-ADP model

The total stress based NGI-ADP model (Grimstad et al. 2012) simulates the soil as elastoplastic, and allows the user to change the orientation of the failure envelope to include anisotropy, using the concept of ADP-zones (Bjerrum 1973) and the principal stress directions. The active (A), direct (D) and passive (P) zones originate from the active and passive earth pressures acting on a sheet pile wall and can be related to similar mechanisms in bearing capacity and slope stability problems, as illustrated in Figure 3.1. Notably, the ADP-concept assumes plane strain conditions, while the NGI-ADP model is implemented for 3D stress space in FE-environment.
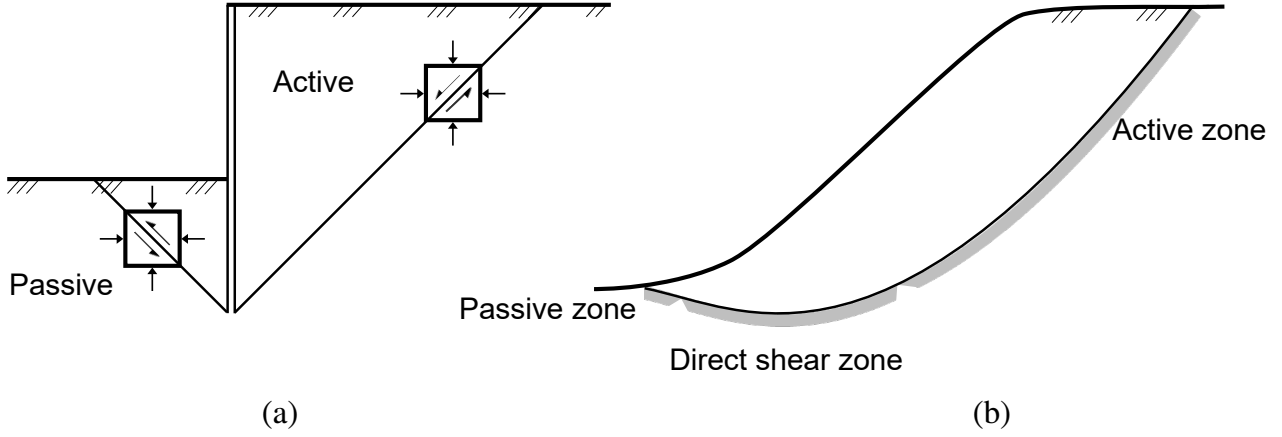
Figure 3.1: *(a) Active and passive earth pressure (Bjerrum 1973) and (b) shearing zones in a slope failure (Skredkommissionen 1995).*

The ADP-zones are a simplification of the complex stress state in a slope, with the three zones being related to direct simple shear tests and triaxial tests in compression and extension, respectively. The important difference between these tests and plane strain tests, is the magnitude of the intermediate stress, σ_2.

The yield criterion is a modification of the classical Tresca formulation:

$$f = \sqrt{H(\omega)\hat{J}_2} - \kappa\frac{s_u^A + s_u^P}{2} = 0 \tag{3.1}$$

where κ is the volumetric hardening parameter, and s_u^A and s_u^P are the undrained shear strengths in active and passive zone, respectively. $\hat{J}_2$ and $\hat{J}_3$ are modified second and third deviatoric invariants described in Paper B-Appendix A and $H(\omega)$ controls the rounding of the Tresca approximation by:

$$H(\omega) = \cos^2\left(\frac{1}{6}\arccos(1 - 2a_1\omega)\right) \tag{3.2}$$

$$\omega = \frac{27}{4}\frac{\hat{J}_3^2}{\hat{J}_2^3} \tag{3.3}$$

where a_1 scales the rounding effect, with $a_1 = 1$ being the exact Tresca formulation. $H(\omega)$ is necessary for rounding the sharp corners of the Tresca formulation, which can create numerical problems in FE simulations. This is however not a problem in limit analyses, as will be discussed in section 7.1. Figure 3.2 illustrates the anisotropic modification and the rounding effect in the deviatoric plane.
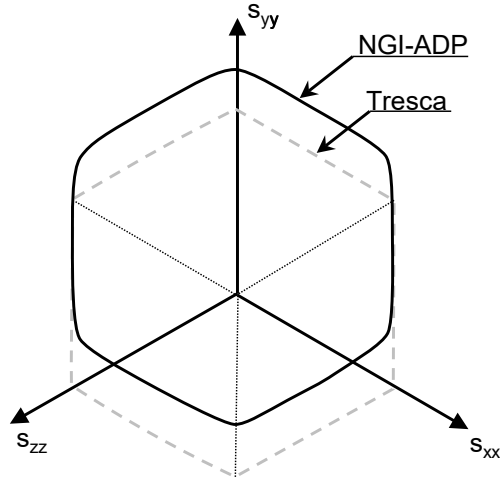
11

Figure 3.2: *Illustration of the difference between yield criterion.*

The model is based on a non-associated flow rule with a non-linear hardening behaviour correlated to the plastic shear strain, γ^p, and the shear strain at failure in triaxial compression, γ_f^C, triaxial extension, γ_f^E and in direct simple shear, γ_f^{DSS}, (Grimstad et al. 2012). As a result of this anisotropic stiffness, the yield surface becomes non-symmetric during plastic loading in FE simulations, which cannot be included in the limit analyses framework.

3.1 Parameter determination

The model consists of four strength parameters; s_u^A, s_u^{DSS} and s_u^P to define the undrained shear strength and the amount of anisotropy from laboratory tests, and $s_{u,inc}^A$ to define the change of undrained shear strength as a function of depth or level. For practical purposes, Grimstad et al. (2012) suggests the undrained shear strength from triaxial tests to be used for the plane strain strength s_u^A and s_u^P, which has been applied in e.g. D'Ignazio et al. (2017), Jostad et al. (2014), Li et al. (2022), and Ukritchon and Boonyatee (2015). Likewise, are the anisotropic strains at failure derived from triaxial tests and direct simple shear tests, as illustrated in Figure 3.3.
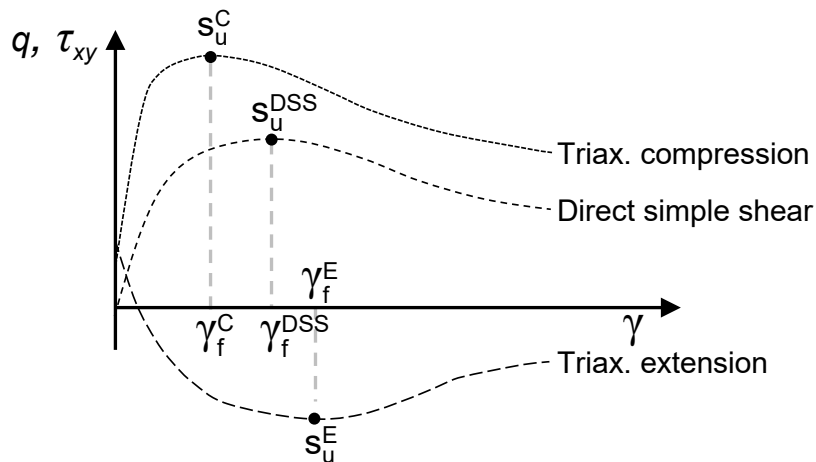

Figure 3.3: *Definition of input parameters for NGI-ADP. Based on D'Ignazio et al. (2017).*

3.2 Critical state constitutive models

The concept of a critical, or ultimate, condition in soil is defined as a state where the soil can experience indefinite plastic shearing without any changes in volume (Schofield and Wroth 1968). In practice, that means that the same (ultimate) behaviour is found independent of drainage conditions, soil state or a loading path (Roscoe et al. 1958). In mean effective stress versus deviatoric stress $(p' - q)$-space, the critical state, cs, is defined as a constant stress ratio, $M = p'_{cs}/q_{cs}$, with a value dependent on the critical state friction angle, φ', in compression, c, and extension, e, respectively:

$$M_c = \frac{6\sin(\varphi')}{3 - \sin(\varphi')} \tag{3.4a}$$

$$M_e = \frac{6\sin(\varphi')}{3 + \sin(\varphi')} \tag{3.4b}$$

M thereby represents the inclination of the Critical State Line (CSL). CSL and the stress history of a clay will dictate its behaviour during plastic loading; a heavily consolidated clay in undrained conditions will dilate and thereby have a reduction of pore pressure until reaching CSL, while a normally consolidated and lightly consolidated clay will instead contract and have an increase in pore pressure before reaching CSL.

One of the major benefits of using CSL as the foundation for a constitutive model is that the stress state of the sample is irrelevant at critical state, including the effects of overconsolidation ratio OCR, coefficient of earth pressure at rest K_0 and any unwelcome sample disturbance. In terms of mobilised strength, the critical state corresponds to the ultimate strength, represented by the constant stress ratio, M, as illustrated in Figure 2.4.

3.3 Stress and strain tensors

A soil element in its natural condition, at a given time step, is subjected to a three-dimensional stress state, which hereafter is referred to as a general stress state. These effective stresses can be described with Cartesian axes (y-axis vertical) using the Cauchy stress tensor, here presented in vector format:

$$\sigma' = [\sigma'_x \ \sigma'_y \ \sigma'_z \ \tau_{xy} \ \tau_{yz} \ \tau_{zx}]^T \tag{3.5}$$

Tensors are presented in vector format throughout this section. The corresponding mean effective stress is then defined as:

$$p' = \frac{1}{3}\left(\sigma'_x + \sigma'_y + \sigma'_z\right) \tag{3.6}$$

From this, the deviatoric stress tensor can be derived:

$$
\boldsymbol{\sigma}'_d =
\begin{bmatrix}
\sigma'_x - p' \\
\sigma'_y - p' \\
\sigma'_z - p' \\
\sqrt{2}\tau_{xy} \\
\sqrt{2}\tau_{yz} \\
\sqrt{2}\tau_{zx}
\end{bmatrix}
=
\begin{bmatrix}
\frac{1}{3}(2\sigma'_x - \sigma'_y - \sigma'_z) \\
\frac{1}{3}(-\sigma'_x + 2\sigma'_y - \sigma'_z) \\
\frac{1}{3}(-\sigma'_x - \sigma'_y + 2\sigma'_z) \\
\sqrt{2}\tau_{xy} \\
\sqrt{2}\tau_{yz} \\
\sqrt{2}\tau_{zx}
\end{bmatrix}
\tag{3.7}
$$

The strain rate tensor is defined analogously to the stress tensor as:

$$
\dot{\boldsymbol{\varepsilon}} = [\dot{\varepsilon}_{xx} \ \ \dot{\varepsilon}_{yy} \ \ \dot{\varepsilon}_{zz} \ \ \dot{\varepsilon}_{xy} \ \ \dot{\varepsilon}_{yz} \ \ \dot{\varepsilon}_{zx}]^T
\tag{3.8}
$$

and the associated deviatoric strain rate tensor:

$$
\dot{\boldsymbol{\varepsilon}}_d =
\begin{bmatrix}
\dot{\varepsilon}_x - \frac{\dot{\varepsilon}_v}{3} \\
\dot{\varepsilon}_y - \frac{\dot{\varepsilon}_v}{3} \\
\dot{\varepsilon}_z - \frac{\dot{\varepsilon}_v}{3} \\
\sqrt{2}\dot{\varepsilon}_{xy} \\
\sqrt{2}\dot{\varepsilon}_{yz} \\
\sqrt{2}\dot{\varepsilon}_{zx}
\end{bmatrix}
=
\begin{bmatrix}
\frac{1}{3}(2\dot{\varepsilon}_x - \dot{\varepsilon}_y - \dot{\varepsilon}_z) \\
\frac{1}{3}(-\dot{\varepsilon}_x + 2\dot{\varepsilon}_y - \dot{\varepsilon}_z) \\
\frac{1}{3}(-\dot{\varepsilon}_x - \dot{\varepsilon}_y + 2\dot{\varepsilon}_z) \\
\sqrt{2}\dot{\varepsilon}_{xy} \\
\sqrt{2}\dot{\varepsilon}_{yz} \\
\sqrt{2}\dot{\varepsilon}_{zx}
\end{bmatrix}
\tag{3.9}
$$

where the volumetric strain rate is defined as:

$$
\dot{\varepsilon}_v = \dot{\varepsilon}_x + \dot{\varepsilon}_y + \dot{\varepsilon}_z
\tag{3.10}
$$

The scalar value of the deviatoric strain rate tensor, used in e.g. simplified triaxial space, is defined by:

$$
\dot{\varepsilon}_d^2 = \frac{2}{3}\{\dot{\boldsymbol{\varepsilon}}_d\}^T\{\dot{\boldsymbol{\varepsilon}}_d\}
\tag{3.11}
$$

3.4 Creep-SCLAY1S

Creep-SCLAY1S is a rate-dependent extension of the well-established elasto-plastic strain hardening model Modified Cam Clay (MCC) (Roscoe and Burland 1968), with a hierarchical structure to account for initial and evolving anisotropy, loss of bonding between particles and the Lode-angle dependency, respectively (Gras et al. 2017; Gras et al. 2018; Sivasithamparam et al. 2015). The model consists of three surfaces when all features are activated, as illustrated in Figure 3.4.
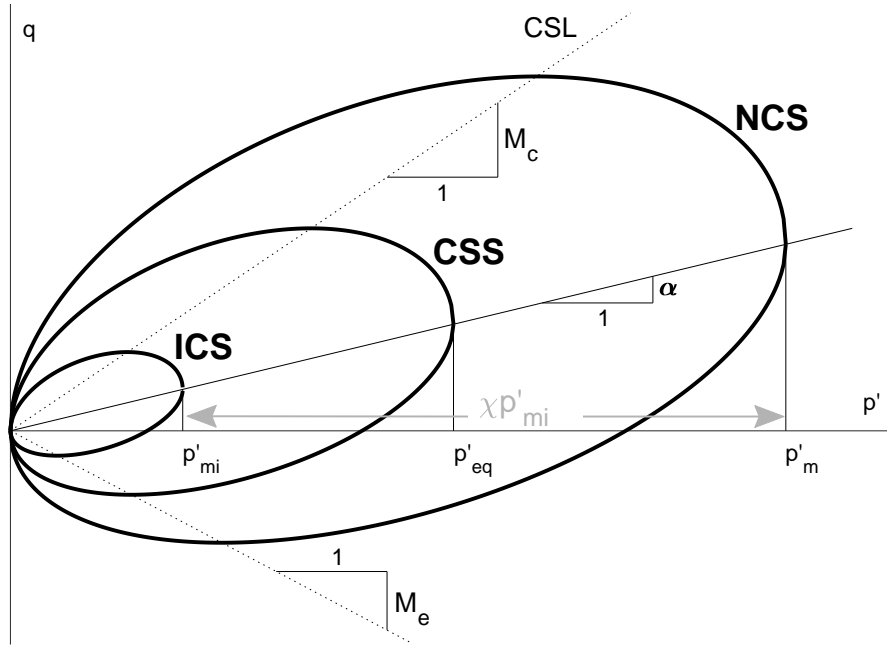

Figure 3.4: *Definition of Creep-SCLAY1S in simplified triaxial space. From Paper C.*

The surfaces, respectively, represent an imaginary Intrinsic Compression Surface (ICS), a Current Stress Surface (CSS) and a Normal Compression Surface (NCS), the latter representing the border between small and large irrecoverable strain increments. ICS, as introduced by Koskinen et al. (2002), represents the imaginary yield surface of an unbonded soil with the same void ratio and fabric orientation as its bonded equivalent. The sizes of the three surfaces are defined by the intrinsic isotropic pre-consolidation pressure p_{mi}, the equivalent mean effective stress p_{eq} and the equivalent preconsolidation pressure p_m, respectively.

Anisotropy and Lode-angle dependency

The orientation and rotation of the surfaces, illustrated by an α-line in Figure 3.4, represent the soil fabric in terms of initial and evolving anisotropy. The fabric orientation and rotation are described by a deviatoric fabric tensor (Sivasithamparam et al. 2015; Wheeler et al. 2003), where a bold symbol implies tensor (in vector format) and a dot over a symbol implies rate, a strain increment

with respect to time:

$$\boldsymbol{\alpha}_d = \begin{bmatrix} \alpha_x - 1 \\ \alpha_y - 1 \\ \alpha_z - 1 \\ \sqrt{2}\alpha_{xy} \\ \sqrt{2}\alpha_{yz} \\ \sqrt{2}\alpha_{zx} \end{bmatrix} = \begin{bmatrix} \frac{1}{3}(2\alpha_x - \alpha_y - \alpha_z) \\ \frac{1}{3}(-\alpha_x + 2\alpha_y - \alpha_z) \\ \frac{1}{3}(-\alpha_x - \alpha_y + 2\alpha_z) \\ \sqrt{2}\alpha_{xy} \\ \sqrt{2}\alpha_{yz} \\ \sqrt{2}\alpha_{zx} \end{bmatrix} \tag{3.12}$$

where the deviatoric fabric tensor components have the property:

$$\alpha_x + \alpha_y + \alpha_z = 3 \tag{3.13}$$

The associated scalar value of the deviatoric fabric tensor is defined by:

$$\alpha^2 = \frac{3}{2}\{\boldsymbol{\alpha}_d\}^T\{\boldsymbol{\alpha}_d\} \tag{3.14}$$

Using the definitions above, the shape of NCS in the general stress space is defined as:

$$f = \frac{3}{2}\Big[\{\boldsymbol{\sigma}'_d - p'\boldsymbol{\alpha}_d\}^T\{\boldsymbol{\sigma}'_d - p'\boldsymbol{\alpha}_d\}\Big] - \Big[\mathrm{M}(\theta)^2 - \frac{3}{2}\{\boldsymbol{\alpha}_d\}^T\{\boldsymbol{\alpha}_d\}\Big](p'_m - p')p' = 0 \tag{3.15}$$

where $\mathrm{M}(\theta)$ is the Lode-angle dependent inclination of the CSL. The shape of ICS and CSS have the same formulation, but instead of p'_m, the size is defined by p'_{mi} and p'_{eq}, respectively. Figure 3.4 illustrates the maximum effect of $\mathrm{M}(\theta)$ on the aspect ratio of the surfaces via inclination in compression, M_c and extension, M_e. The non-circular shape in the deviatoric plane, dependent on the ratio $m = M_e/M_c$, is shown in Figure 3.5.
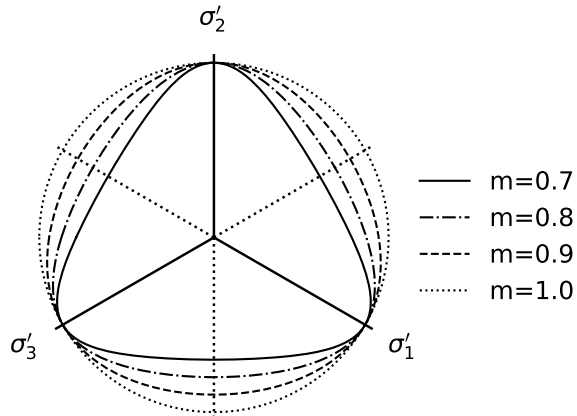

Figure 3.5: *Illustration of Lode angle dependency in the deviatoric plane.*

16

The incorporation of M(θ) in Creep-SCLAY1S (Sivasithamparam et al. 2015) is based on the formulation by Sheng et al. (2000):

$$M(\theta) = M_c \left(\frac{2m^4}{1 + m^4 + (1 - m^4) \sin 3\theta_\alpha} \right)^{\frac{1}{4}} \tag{3.16}$$

where:

$$\sin 3\theta_\alpha = - \left[\frac{3\sqrt{3}}{2} \frac{(J_3)_\alpha}{(J_2)_\alpha^{\frac{3}{2}}} \right] \tag{3.17}$$

Here, the second $(J_2)_\alpha$ and third $(J_3)_\alpha$ invariants are based on the modified deviatoric stress $(\sigma' - \alpha_d p')$ to include the fabric orientation (Sivasithamparam et al. 2015).

The initial anisotropy of a K_0 consolidated clay is represented by a scalar value, α_0, while the evolving anisotropy due to irrecoverable strains results in changes in the components of α_d via a separate rotational hardening law (Wheeler et al. 2003):

$$\dot{\alpha}_d = \omega \left[\left(\frac{3\sigma'_d}{4p'} - \alpha_d \right) \langle \dot{\varepsilon}_v^c \rangle + \omega_d \left(\frac{\sigma'_d}{3p'} - \alpha_d \right) \dot{\varepsilon}_d^c \right] \tag{3.18}$$

where $\dot{\varepsilon}_v^c$ denotes the volumetric viscoplastic strain rate and $\dot{\varepsilon}_d^c$ is the deviatoric counterpart. The Macaulay brackets, $\langle \ \rangle$, mean that $\langle \dot{\varepsilon}_v^c \rangle = \dot{\varepsilon}_v^c$ for $\dot{\varepsilon}_v^c \geq 0$ and $\langle \dot{\varepsilon}_v^c \rangle = 0$ for $\dot{\varepsilon}_v^c < 0$. ω and ω_d represent the absolute and relative effectiveness of rotational hardening, respectively. Whilst the value for ω_d can be theoretically derived, the value for ω needs to be calibrated against experimental data (Gras et al. 2018).

Given the hierarchical structure of Creep-SCLAY1S, an assigned initial anisotropy of $\alpha_0 = 0$ simply reverts the model to isotropic in terms of yielding. If in addition $\omega = 0$, the rotational hardening law is deactivated and the anisotropy becomes fixed to its initial value, as illustrated in Figure 3.6. It should be noted how the surface shape is consistently governed by the critical state lines.
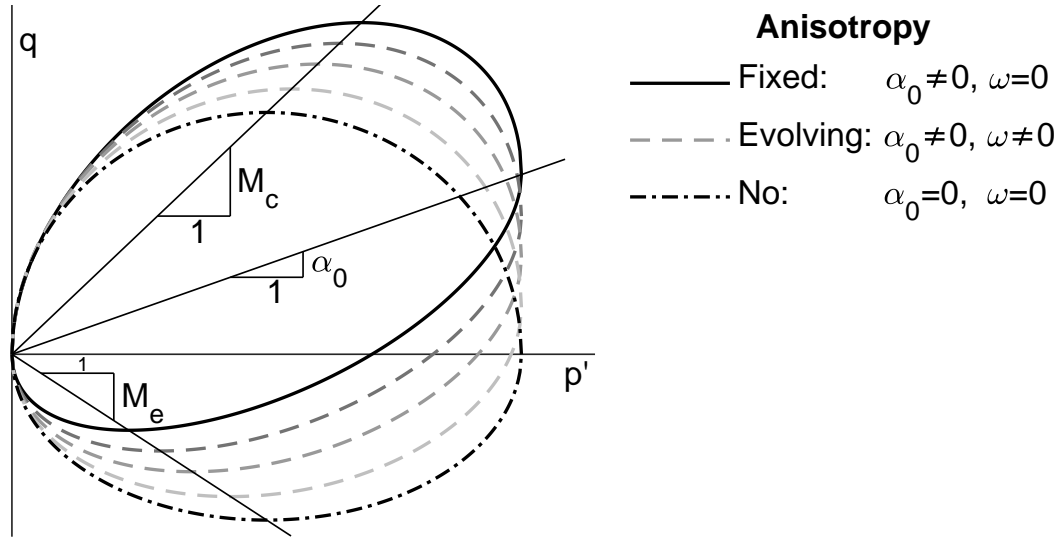
Figure 3.6: *Initial surface orientation and evolving surface rotation, with Lode-angle dependency. Adapted from Paper D.*

The resulting effect of initial and evolving anisotropy on the mobilised shear strength in the complex stress state in a slope is further examined in Paper D.

The conversion of the initial scalar value α_0 to $\boldsymbol{\alpha}_d$ requires the assumption of one-dimensional loading history. By assuming horizontal soil stratification, applying Jaky's formula $K_0^{nc} = 1 - \sin(\varphi')$ (Jaky 1948) for a normally consolidated soil and assuming cross-anisotropy, α_0 is derived from the critical state friction angle at triaxial compression, φ' (Wheeler et al. 2003). A full derivation of the initial deviatoric fabric tensor from α_0 is found appended in Paper C.

Effect of bonding

The post-peak softening behaviour seen in sensitive clays, as a result of degradation of bonds, is accounted for in the model using a separate hardening law, called destructuration law (Koskinen et al. 2002) inspired by the idea of Gens and Nova (1993). The amount of bonds between particles, χ, is used to scale the size of the bonded NCS in relation to its (unbonded) counterpart ICS:

$$p'_m = (1 + \chi)p'_{mi} \tag{3.19}$$

as illustrated in Figure 3.4. The destructuration law governs the rate of the degradation during viscoplastic straining:

$$\dot{\chi} = -\xi\chi\left(|\dot{\varepsilon}_v^c| + \xi_d\dot{\varepsilon}_d^c\right) \tag{3.20}$$

where ξ and ξ_d are model parameters that control the rate of the degradation, see e.g. Gras et al. (2018). An indication of the initial amount of bonding, χ_0, is given by the sensitivity, S_t, by:

$$\chi_0 = S_t - 1 \tag{3.21}$$

Again, this addition to the MCC model can be switched off by assigning $\chi = 0$. It should also be noted that the fabric anisotropy, $\boldsymbol{\alpha}_d$, is independent of the bonding.

Volumetric hardening

The change in the size of (the unbonded) ICS, and hence also NCS, during viscoplastic straining is controlled by the volumetric hardening law similar to the formulation in MCC model:

$$\dot{p}'_{mi} = \frac{p'_{mi}}{\lambda_i^* - \kappa^*} \dot{\varepsilon}_v^c \qquad (3.22)$$

where λ_i^* is the modified intrinsic compression index and κ^* is the modified swelling index.

Rate-dependency and visco-plastic strains

The total strain rate is defined analogously to the MCC model:

$$\dot{\varepsilon} = \dot{\varepsilon}^e + \dot{\varepsilon}^c \qquad (3.23)$$

with the creep component above simply replaced with its plastic equivalent when rate-dependency is excluded, as defined in e.g. Wheeler et al. (2003) and Koskinen et al. (2002). The magnitude of the creep strains is dictated by the relation between the Normal Compression Surface (NCS) and the Current Stress State (CSS) in Figure 3.4, i.e. the generalised overconsolidation ratio, OCR*:

$$OCR^* = \frac{p'_m}{p'_{eq}} \qquad (3.24)$$

This ratio is used in a viscoplastic multiplier, $\dot{\Lambda}$ (Grimstad et al. 2010), applied for Creep-SCLAY1S as (Sivasithamparam et al. 2015):

$$\dot{\varepsilon}_{ij}^c = \dot{\Lambda} \frac{\delta p'_{eq}}{\delta \sigma'_{ij}} \qquad (3.25)$$

$$\dot{\Lambda} = \frac{\mu_i^*}{\tau_{ref}} \left(\frac{p'_{eq}}{p'_m} \right)^\beta \left(\frac{M_c^2 - \alpha_{K_0^{nc}}^2}{M_c^2 - \eta_{K_0^{nc}}^2} \right) \qquad (3.26)$$

$$\beta = \frac{\lambda_i^* - \kappa^*}{\mu_i^*} \qquad (3.27)$$

where the first term of $\dot{\Lambda}$, is a constant viscoplastic rate, namely the ratio of the modified intrinsic creep index, μ_i^*, over the reference time, τ_{ref}. This term is scaled by the relation between CSS and NCS, i.e. the inverse of OCR* (second term). $\dot{\Lambda}$ is thereby very sensitive to the degree of overconsolidation. The third term is included to ensure compatibility for oedometric conditions.

Both τ_{ref} and p'_m, and therefore also the size of NCS, are dependent on the loading rate in an oedometer test. By assuming that creep roughly always exists during a loading step when OCR≤1, the reference time can be assumed to be equal to the duration of a loading step, as discussed by Leoni et al. (2008).

Notably, the definition of the viscoplastic multiplier implies that there is no pure elastic region, which is in line with the experimental observations (Yin et al. 2011), but deviates from Perzyna's overstress theory (Perzyna 1966). As a result, the determination of the model parameters is straightforward, by linking a reference time to the apparent preconsolidation pressure derived from test results (Leoni et al. 2008). The drawback is that the creep definition also allows for OCR* <1, which in practice results in (unrealistically) large creep rates.

Framework from Modified Cam Clay model

The (isotropic) elastic response in the SCLAY-family of models stems from the formulation of the MCC model:

$$\dot{\varepsilon}^e_{ij} = \frac{1}{3K'}\dot{p}'\delta_{ij} + \frac{1}{2G'}\dot{\sigma}_{d,ij} \quad \text{with} \quad \delta_{ij} = \begin{cases} 1 & i = j \\ 0 & i \neq j \end{cases} \tag{3.28}$$

where $K' = p'/\kappa^*$ refers to the effective elastic bulk modulus, with κ^* as the modified swelling index. The effective elastic shear modulus, $G' = 3K'(1 - 2\nu')/2(1 + \nu')$ is assumed to have a constant value of Poisson's ratio, ν'.

Lastly, just like the MCC model, the SCLAY-family assumes associated flow, in the lack of evidence to the contrary (Karstunen and Koskinen 2008), and for the sake of simplicity (Wheeler et al. 2003).

3.4 Parameter determination

A FE simulation using Creep-SCLAY1S requires values for 10 model parameters, in addition to 4 parameters relating to the initial state. 11 of these parameters can be directly derived from laboratory tests, and the remaining three need to be calibrated in FE triaxial test simulations. Table 3.1 summarises the necessary laboratory tests, and the related soil parameters. The rows in roman style are soil constants, which are independent of the state of the soils, while *italic text* refers to initial state variables.

Table 3.1: *Summary of model parameters in Creep-SCLAY1S and how they are derived. Text in italic highlights the four state variables.*

FALL CONE TEST	*Initial amount of bonding, χ_0 (Estimation)*
OEDOMETER TEST	Modified intrinsic compression index, λ_i^*
	Modified swelling index, κ^*
	Poisson's ratio, ν'
	Modified intrinsic creep index, μ_i^*
	Reference time, τ_{ref}
	Pre-overburden pressure, POP, or overconsolidation ratio, OCR
UNDRAINED TRIAXIAL TEST(S)	Stress ratio at critical state in triaxial compression, M_c
	Stress ratio at critical state in triaxial extension, M_e
	Initial value of anisotropy, α_0, derived from M_c (See text)
	Relative rate of rotational hardening due to deviatoric strains, ω_d, derived from M_c
MODEL CALIBRATION	Absolute rate of rotational hardening, ω
	Absolute rate of destructuration, ξ
	Relative rate of destructuration due to deviatoric strains, ξ_d

The initial amount of bonding, χ_0, can be estimated from S_t from fall cone tests using Equation 3.21, while the soil parameters from oedometer tests are graphically derived as shown in Figure 3.7. The reference time, τ_{ref}, is equal to the time interval for load steps in oedometer tests, typically 1 day, as previously discussed.
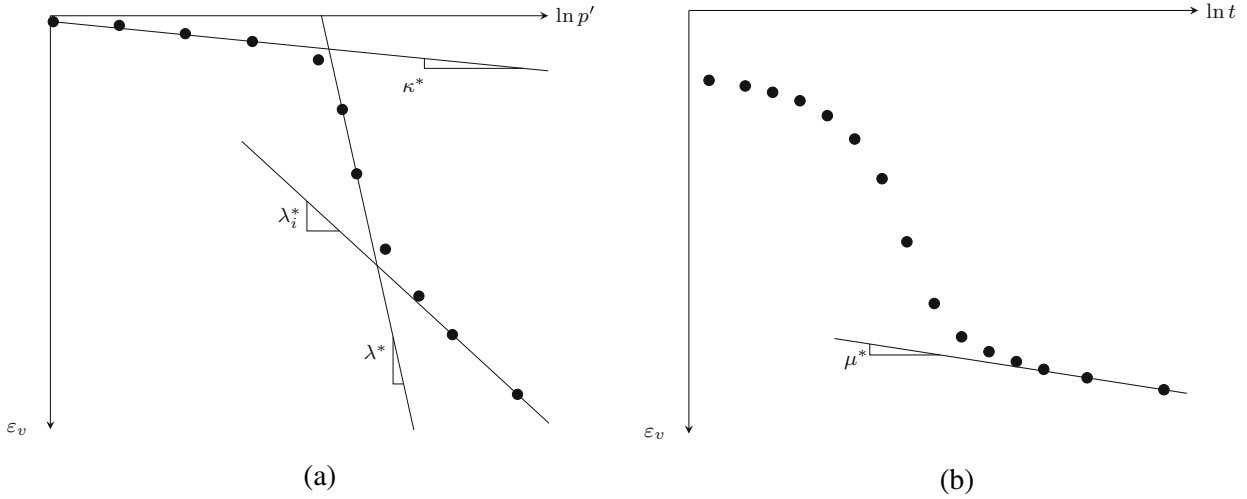
Figure 3.7: *Definition and differentiation between (a) λ^*, λ_i^* and κ^* and (b) μ_i^* from oedometer test. $\mu^* = \mu_i^*$ for sufficiently high stress or for reconstituted samples when all structure is erased. From Gras et al. (2018).*

Both α_0, the subsequent $\boldsymbol{\alpha}_d$, and ω_d are derived from M_c assuming one-dimensional consolidation history using Jaky's formula (Jaky 1948) and cross-anisotropy (Wheeler et al. 2003), which should be reflected in the initial state in the FE simulation. This is further discussed in Paper C and Paper D.

Lastly, the model parameters ω and ξ have empirical boundaries based on the compressibility of the soil, i.e λ_i^* and κ^*, and χ_0 (Gras et al. 2018). When destructuration is excluded, the permissible range of ω is instead governed by the non-intrinsic λ^* with κ^*. For ξ_d, it can be assumed that influence of the deviatoric creep strains never exceeds the volumetric creep strains, i.e. $0 \leq \xi_d \leq 1$.

4 Methods for slope stability analysis

4.1 Limit Equilibrium Method

The Limit Equilibrium Method (LEM) is the most commonly used method for slope stability assessment with over a century of history, starting with Hultin (1916), via Bishop (1955) and Janbu (1954) up to the current well-known Morgenstern and Price (1965) and Spencer (1967). The concept of LEM is based on a pre-defined sliding mass that is discretised into vertical slices for which force and/or moment equilibrium is calculated for each slice and the total mass. Notably, the latter two also account for interslice normal forces and interslice shear forces, thereby satisfying both force and moment equilibrium for each slice, but with the need of iterations to find the resultant of the interslice forces. Figure 4.1 illustrates the iterative procedure, with λ_{LEM} defined as the scaling factor of the interslice resultant and the Factor of Safety, defined as the ratio of the available shear strength along the slip surface over the shear stress for the same surface.
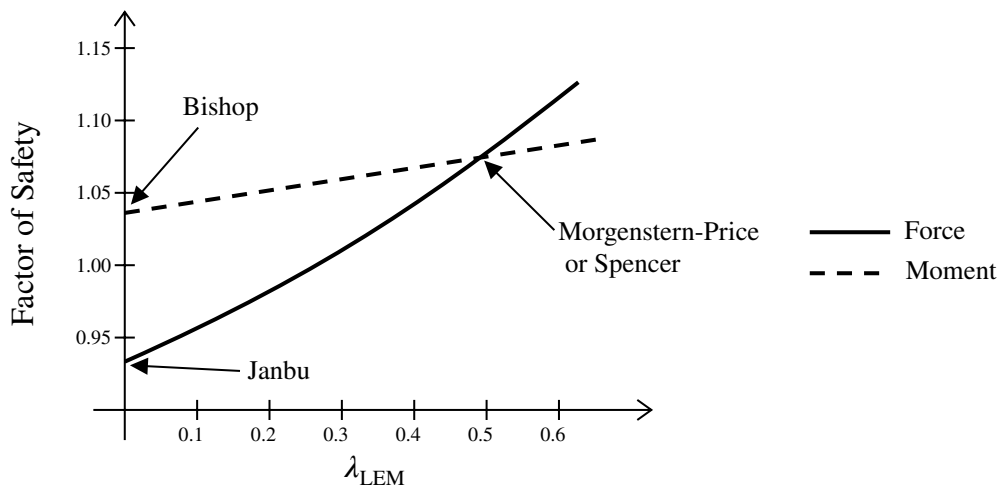

Figure 4.1: *Comparison of methods of slices with respect to equilibrium conditions, from Krahn (2003).*

The benefit of LEM is its simplicity and computational efficiency. The simplicity does however come with the drawbacks: (i) a user- and pre-defined slip surface (ii) the assumption of a constant mobilisation of the shear strength along the shear band, implying that the same value of the shear strength is mobilised regardless of the magnitude of strains (Duncan and Wright 1980) (iii) the limited options to include anisotropy and non-existing options to account for changes in soil response (softening, hardening, changes in anisotropy) that affect the mobilised strength.

4.2 Discontinuity Layout Optimization

Discontinuity Layout Optimization (DLO) (Smith and Gilbert 2007) is an upper bound limit analysis that disrectises the soil mass into discontinuities (slip-lines), which result in a large number of individually moving blocks. Similar to LEM, the equilibrium is dictated by the shearing between the blocks, while DLO is based on kinematics, rather than (stress) equilibrium. The obtained failure mode is thereby the combination of slip-lines with the least dissipated energy, with

23

a safety factor defined as the ratio of the rate of work due to external loads over the simultaneous work done by internal stresses (Smith and Gilbert 2007).

The method is implemented in the software LimitState:GEO (LimitState 2021), with a summary of the optimisation technique in Figure 4.2. The user assigns a nodal density in Figure 4.2a, of which the software generates node-to-node slip-lines. Out of efficiency, the slip-lines are either restricted to adjacent nodes (Figure 4.2b) or to all nodes (Figure 4.2c), depending on the extent of the problem. The obtained (low accuracy) solution is used as input for searching all potential slip-lines, to find the ones that violate the failure criterion. Only the slip-lines that violate the failure criterion will be added to the problem, followed by a new computation of the upper bound solution. This iterative, adaptive method is continued until no more slip-lines are added. The final combination of slip-lines is then subject for the safety analysis by either (i) strength reduction, or (ii) increase of gravity, to identify the combination of slip-lines that have the lowest (kinematic) safety factor, illustrated in Figure 4.2d.
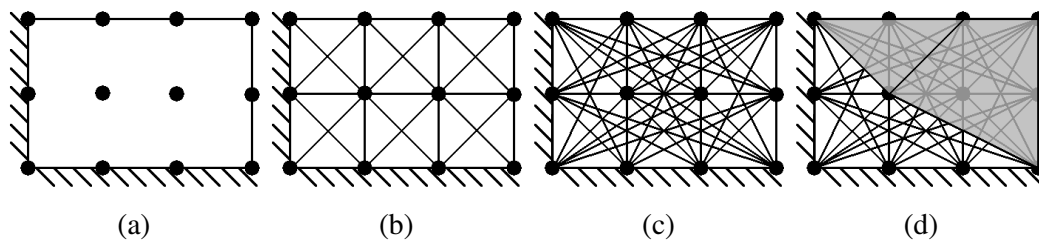

| (a) | (b) | (c) | (d) |

Figure 4.2: *Stages of (a-c) discretisation and (d) calculation of soil mass in DLO. From Paper B, based on Gilbert et al. 2010.*

DLO has the advantage of automatically discretising the whole soil mass in search of the critical failure mode, while maintaining low computational time. The use of (infinitely thin) slip-lines also circumvents any mesh-dependent shear band width, in contrast to e.g. FE-based methods. The drawback of using linear slip-lines is, however, the default restriction to translational slips of the individual blocks, which require a relatively high nodal density to simulate global rotational failure, as illustrated in Figure 4.3. The use of limit analysis also restricts the soil behaviour to perfectly-plastic with a constant mobilised shear strength for each slip line. Both of these drawbacks are also valid for LEM, while DLO, with its generalised search of failure mode, is indeed an interesting intermediate step between LEM and FE analysis.
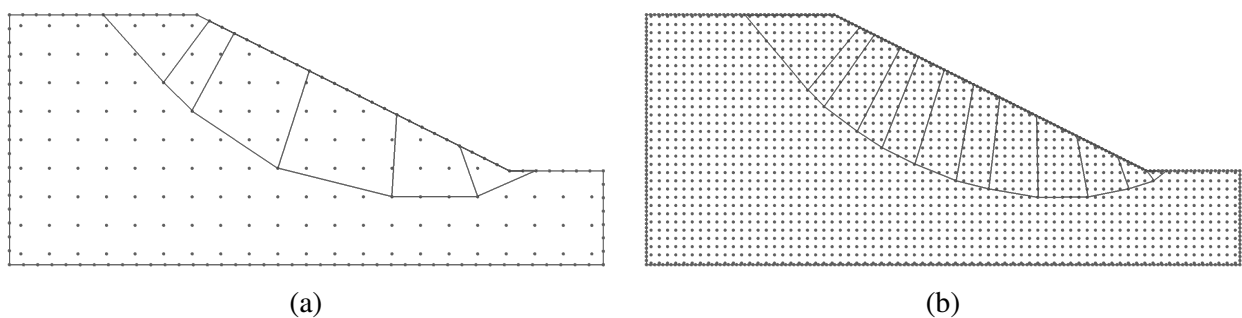

| (a) | (b) |

Figure 4.3: *Examples of discontinuities at failure for (a) coarse nodal density and (b) very fine nodal density.*

4.3 Finite Element Limit Analysis

Finite Element Limit Analysis (FELA) implements both the lower bound theorem (static equilibrium) and upper bound theorem (kinematic equilibrium) separately, for a soil mass discretised into a mesh of elements (Sloan 2013). The use of finite elements allows the inclusion of stress history, with the resulting (effective) stress state used as input for the safety analysis. FELA performs the safety analysis separately for each theorem and the resulting discrepancy between the upper and lower bound solution can be reduced by an increase of mesh density.

The method is implemented in the software Optum G2 (Krabbenhoft 2016), where the safety factor and failure mode are determined analogously to DLO, by either: (i) strength reduction or (ii) increase of gravity. The software also allows for mesh adaptivity, as illustrated in Figure 4.4, which is a neat solution to both reduce the discrepancy in safety factor between upper and lower bound solution and reduce the inherited problem of mesh-dependent shear band width.
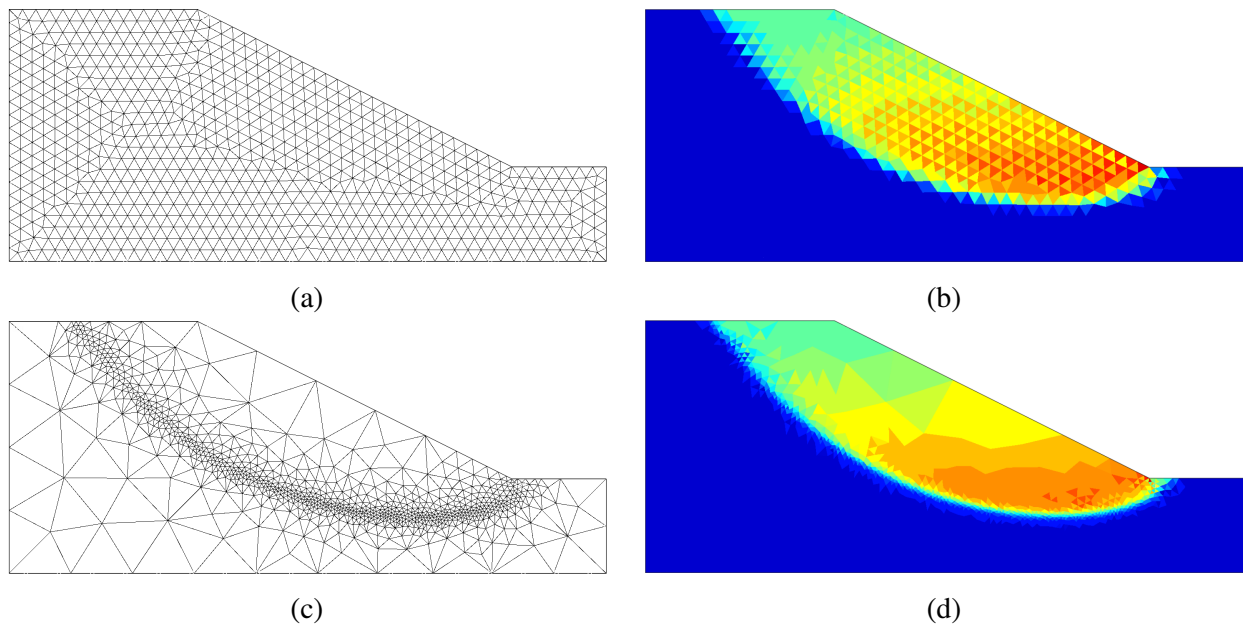

| (a) | (b) |
| (c) | (d) |

Figure 4.4: *Examples of results using FELA; (a-b) without mesh adaptivity and (c-d) with mesh adaptivity. Colour grading represents horizontal displacement.*

FELA is a simple yet rigorous method for determining the safety factor and failure mode, with the advantage of including stress history and no *a-priori*-assumptions of the failure mechanism. The limit analysis framework, assuming perfectly-plastic soil behaviour, does however limit the use of advanced soil models and simulations of changes in soil response, just as in DLO, but nevertheless the method is an advancement to LEM.

4.4 Finite Element Method

A Finite Element (FE) analysis divides the soil mass into a mesh consisting of elements, where the response of each element is computed based on input data and the interaction with the surrounding elements. The latter means that both static and kinematic conditions are fulfilled simultaneously. Both failure mode and the safety factor are based on (numerical) non-convergence in the calculation

model. This non-convergence originates from the incapability of the numerical procedure to find equilibrium in the model. However, that cannot be distinguished from numerical instabilities in the model (Utili and Crosta 2015) which requires a visual inspection of the output to ensure the development of a slip surface.

Practically, the failure mode occurs where the mobilised shear strength is lower than the applied shear stress, as a result of the soil model and its response to the (effective) stress state. Figure 4.5 illustrates how the elements deform and interact, in particular in contrast to FELA in Figure 4.4.
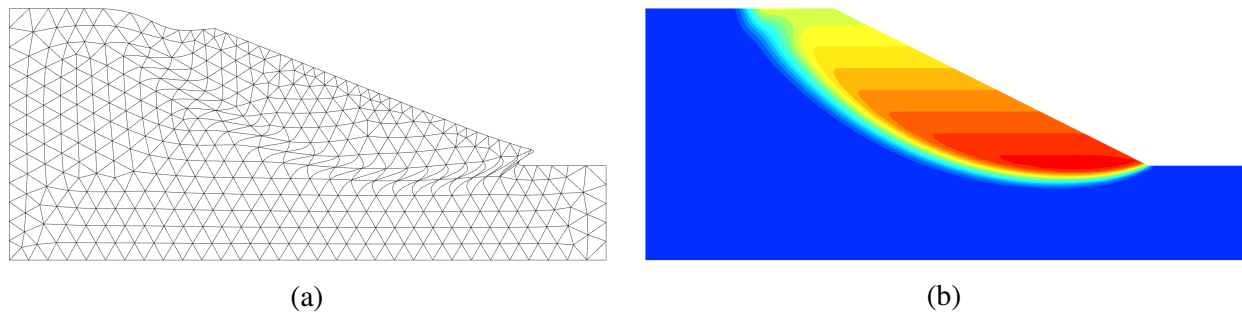

| (a) | (b) |

Figure 4.5: *Examples of (a) deformed mesh from FEM and (b) the interpolation between elements, here represented by horizontal displacements. Colour grading represents horizontal displacements.*

The safety analysis in FEM is performed either as (i) strength reduction (Brinkgreve and Bakker 1991; Zienkiewicz et al. 1975) or (ii) increase of gravity (Chen and Mizuno 1990). The implementation of the latter varies with FE software, but this thesis is limited to the use of PLAXIS (PLAXIS bv 2021). The strength reduction is integrated in PLAXIS software for the standard models, and uses the cohesion intercept, c', and/or the friction angle, φ', as input parameters for the soil model, and is thus not compatible with e.g. soil models sprung from Modified Cam Clay. The use of gravitational increase in effective stress analysis can however increase the strength of the soil, particularly in combination with non-cap models such as Mohr-Coulomb, and potentially create unrealistically high safety factors for shallow slopes (Hu et al. 2019; Swan and Seo 1999).

The overall strength of FEM for safety analysis is the ability to include transient effective stress states in combination with advanced soil models. As so, changes in effective stresses and the corresponding soil response in a slope, including the mobilised strength, can be varied both spatially and as a function of time. This comes with the cost of long computational times, with a safety factor being very sensitive to not only the numbers of elements in the discretisation, but also to the precision of the iterative procedure, since these dictate when the individual stress path reaches the failure criterion. The FE model thereby has apparent limitations also in 2D-3D(-4D) geometry and/or mesh density.

4.5 Comments on full-scale modelling

Validation of slope stability analyses is difficult, as there are virtually no cases where a natural slope in sensitive clay has been brought to failure in a controlled manner. The behaviour of natural slopes, as created by erosion processes, is however expected to bear some similarities with the behaviour of cut slopes (Leroueil 2001).

One of the few cases of full-scale test excavations brought to failure was performed in Champlain Sea clay, so-called Leda clay, in Mont-Saint-Hilaire, Canada. Lafleur et al. (1988) showed that failures in relatively steep cuts (34° and 45°) were both preceded by minor shallow slides, typically to be found using effective stress analysis with Mohr-Coulomb as soil model. Yet, as the failures occurred within a week from the start of the excavation, an undrained soil behaviour might have been expected. Stability calculations performed with LEM using effective- and total stress analyses (Lafleur et al. 1988), respectively, showed that the effective stress analyses gave the best estimate of the safety factor. The total stress analyses, using peak strength values, resulted in an overestimation of the stability. Although a steady-state pore pressure situation was reached after 5 months, all failures within the test site occurred well before that, confirming that the stability of slopes is indeed a time-dependent, coupled hydromechanical problem and should be simulated as one.

5 New methodologies: overview

The process of numerical modelling of slope stability can be summarised in Figure 5.1. Disregarding any human activities, the soil at any geological site not only has inherent geological variability, but also evolving soil properties that originate from e.g. time-, temperature- and effective stress based changes.
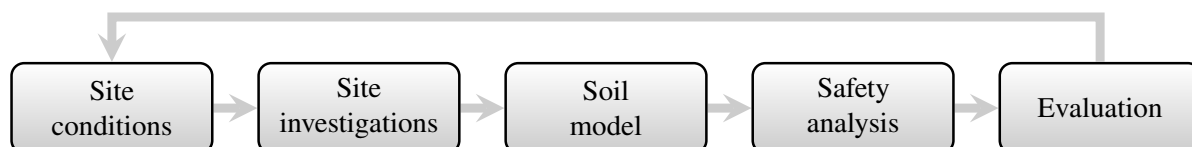

Figure 5.1: *Conceptual steps of slope stability assessment. Inspired by Leroueil and Locat (1998) and Phoon and Kulhawy (1999).*

Sampling and re-occurring in-situ measurements will therefore provide snapshots with point-specific data, with varying quality and quantity. As discussed by Christian et al. (1994) and Phoon and Kulhawy (1999), each measurement has a built-in error stemming from the test procedure, execution and transformation from measurement to geotechnical soil property. These interpreted soil properties serve as input to a soil model to simulate the soil behaviour at element-level, which in turn serves as input to system-level modelling of the safety and expected failure mode of a slope.

The outcome thereby consists of several steps of idealisation, assumptions and accumulated errors, which are compensated by applying a safety margin on the result. For practical engineering purposes, this safety margin is related to the consequence of a slope failure and the amount and reliability of the site investigations (Frank et al. 2015), focusing on the first two boxes in Figure 5.1. Less attention has been drawn to the choice of soil model and the computational tools available, as discussed by Fenton and Griffiths (2008), to include more advanced soil behaviour in slope stability analyses, which is the focus of this thesis. The work consists of three parts, summarised in Figure 5.2.
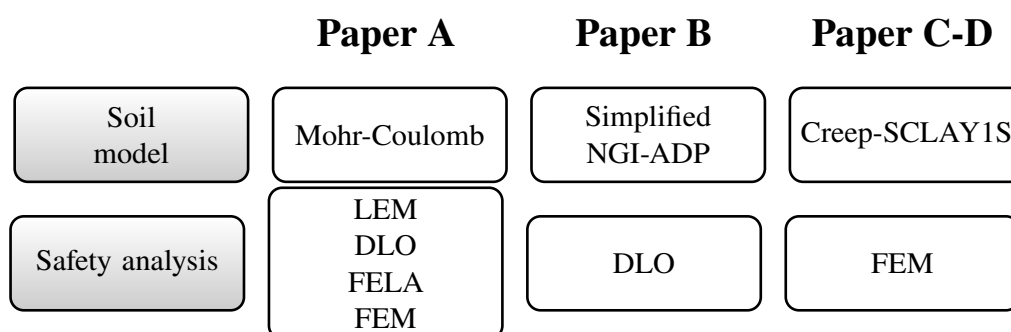

Figure 5.2: *Summary of the methodologies in appended papers.*

Paper A

Paper A consist of a comparative study of the effect of calculation method on the predicted failure mode and safety factor using the Mohr-Coulomb failure criterion. The chosen soil model is commonly used for slope stability assessment, given its simplicity and inclusion of effective stresses. The soil model is applied in LEM, DLO, FELA and FEM on a benchmark slope, both for total- (equivalent to Tresca failure criterion) and effective stresses. For total stress analyses, all the methods resulted in almost identical failure modes.

In the case of effective stress analyses, however, the choice of calculation method surprisingly affects both failure mode and safety factor. In addition, LEM and DLO give the least conservative results (the highest safety factor) which implies the need of consideration of other methods for safety- and critical cases. This low-level complexity in both soil model and safety analysis (Figure 5.1) is appealing due to short computational times, but such approaches clearly lack in precision, and at the same time neglect the evolving effective stress state in the soil and the subsequent effect on state parameters, such as anisotropy.

Paper B

Paper B gives an introduction to a simplified version of the anisotropic, total stress based NGI-ADP model in the DLO software LimitState:GEO. In limit analysis framework, the NGI-ADP model is condensed to a failure criterion, i.e. simulating perfectly plastic behaviour. This research implementation was compared with the full NGI-ADP implementation in PLAXIS 2D, with the results generally showing good agreement with respect to safety factor and failure mode. The study is one of the few that compare DLO and FEM for slope stability assessment and highlight the potential of using DLO for a more robust approach to safety analysis than LEM. The use of a simplified NGI-ADP model in DLO is an advancement from the user-defined methods in LEM since it allows for a fixed anisotropy with a subsequent computational efficiency. Referring to Figure 5.1, the study successfully adds complexity to both the constitutive model and safety analysis, yet still results in a safety factor comparable to the traditional LEM.

Paper C

Paper C gives an introduction of an elasto-viscoplastic constitutive model for the use in slope stability context. The rate-dependent Creep-SCLAY1S model allows for both initial and evolving anisotropy, in addition to post-peak softening characteristics for sensitive clay. Given the mathematical assumptions, a slope stability assessment of a natural slope using the model requires simulation of the geological (unloading) process from horizontal ground surface to its current slope geometry. The advantage lies in the ability to simulate the complex state of the soil within a natural slope, including stress rotations and the subsequent fabric rotations (anisotropy), although the user only provides the soil parameters for the horizontal ground.

The subsequent safety analysis is able to reproduce the failure mechanism obtained from total stress analyses in Paper A, by increasing the gravity in the model to generate excess pore pressure until failure occurs. The concept of a safety factor is however non-trivial when using a rate-dependent soil model, since the safety factor would not only be rate-dependent, but also dependent on the assigned rate of gravity that induce the failure. Relating to Figure 5.1, the high complexity in the constitutive model offers the possibility to simulate various site conditions with limited, but well-planned, in-situ measurements. However, the high complexity comes at the expense of more

demands on the user; in terms of time and knowledge for setting up the model and relating the results to a conventional safety framework.

Paper D

A study of the effect of (i) fixed (initial) anisotropy (ii) evolving anisotropy and (iii) destructuration on the stability and failure mode when using the rate-dependent Creep-SCLAY1S model. Since the model is hierarchically formulated, anisotropy and destructuration can be switched on/off separately. Given the same unloading process and a constant application rate of gravity in the safety analysis, all three cases affect the failure mode and the ultimate gravity at failure. This was expected for the anisotropy, but the varying results using destructuration highlight its influence on the progression of the failure. Ultimately, initial and evolving anisotropy, and destructuration, are all three of importance for the safety analysis when using Creep-SCLAY1S, to account for the spatially varying effective stress distribution and the corresponding soil response. The study confirms that the high-level complexity in Creep-SCLAY1S is indeed necessary to be able to understand the soil response in a natural slope.

6 Description of benchmark slope

A representative site along Göta River with large deposits of sensitive clay was chosen to illustrate the applicability of different methods of slope stability assessment in Paper A, C and D. The site is located 13 km north of Gothenburg, in the Göta River valley, see Figure 6.2, which is one of the most landslide prone areas in Sweden (SGI 2012). The site was extensively investigated during the planning and design process of a new motorway and high-speed railway in the area (BanaVäg i Väst) (Karlsson and Karstunen 2017). Both soil properties and slope geometry are taken from the site, whereas the hydrological conditions and geometry of the riverbed are hypothetical to simulate a marginally stable slope. The presence of any (thin) dry crust is excluded to avoid that affecting the results. Figure 6.2 illustrates the assumed geometrical conditions, with the pore pressure head located 1 m below the surface at the slope crest. The assigned soil properties for Mohr-Coulomb and Creep-SCLAY1S are found in Paper A and Paper B, respectively. Results from index tests (points) and triaxial tests (black outline) are shown in Figure 6.3.
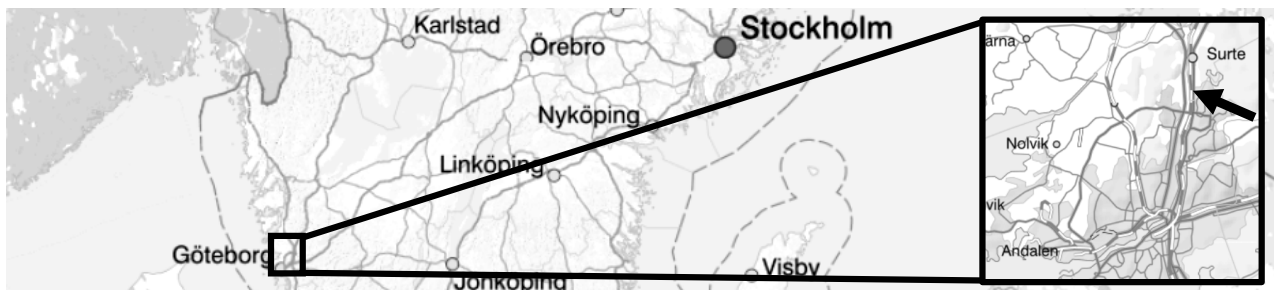

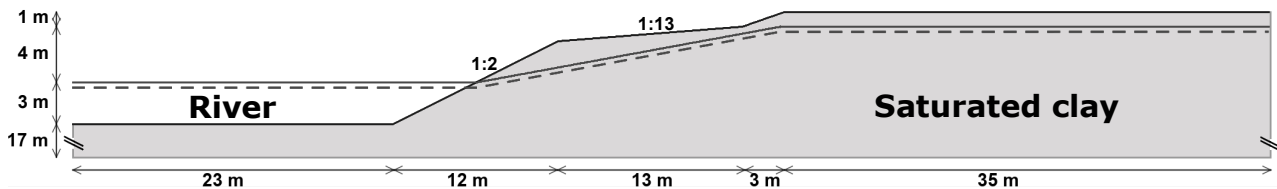Figure 6.1: *Location of geological site. Adapted from Paper A.*

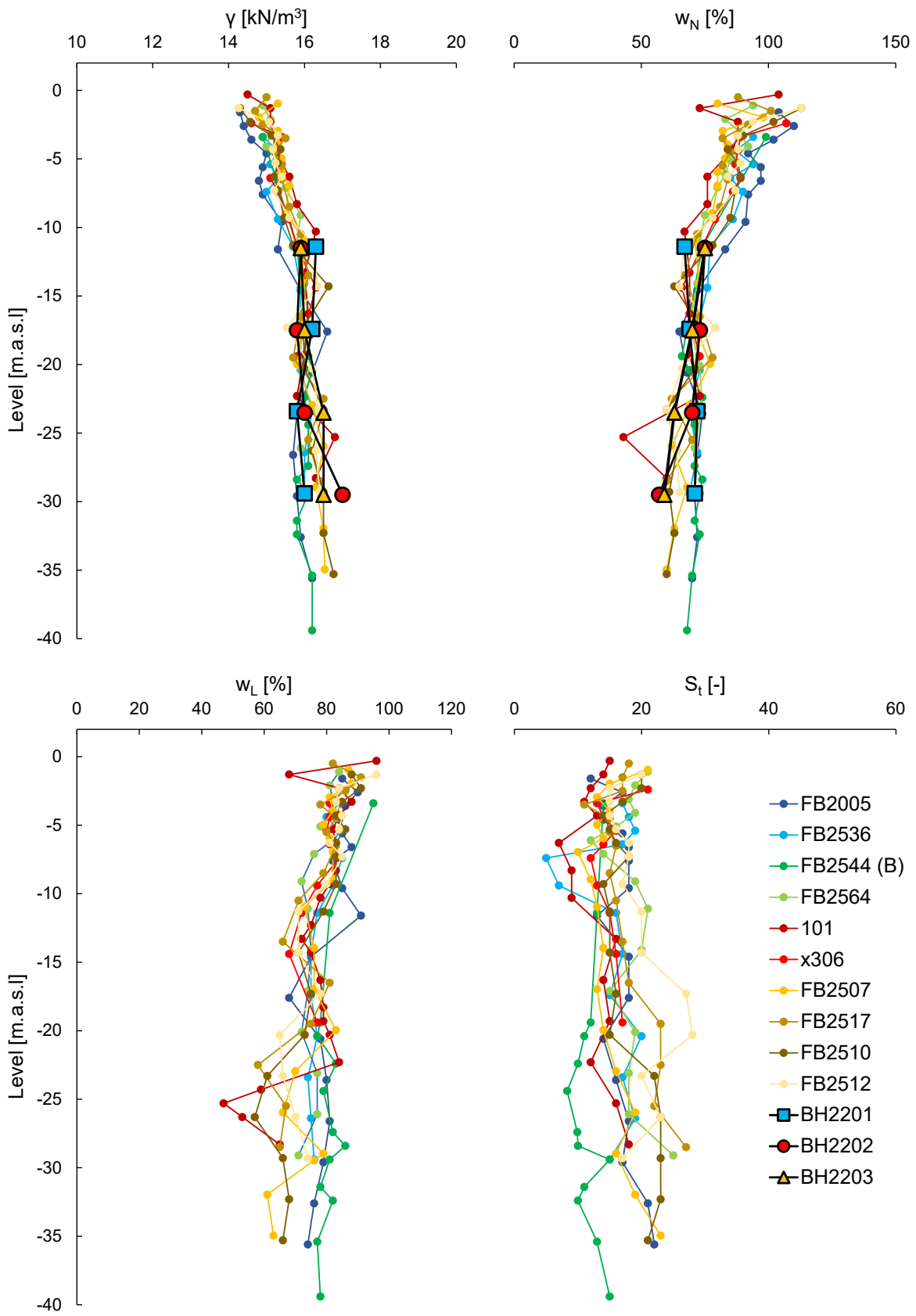Figure 6.2: *Slope geometry. Adapted from Paper B.*

Figure 6.3: *Unit weight, γ, natural water content, w_N, liquid limit, w_L, and sensitivity, S_t, from samples taken from the site.*

7 Methodologies

7.1 Simplified NGI-ADP model in DLO

The upper bound limit analysis method DLO, as implemented in LimitState:GEO, has previously been restricted to isotropic material models. DLO itself is an interesting intermediate step between the conventional LEM and the more demanding FEM, since it offers a discretisation of the whole soil mass, while applying a computationally simple and efficient theoretical framework with consistent accuracy. The soil model NGI-ADP, on the other hand, is an anisotropic model with straightforward input to be extracted from conventional laboratory tests. The NGI-ADP constitutive model cannot be implemented in LimitState:GEO as a whole, given the Limit Analysis framework, but is instead condensed to a failure criterion.

Previous verification of DLO for slope stability problems has been focused on LEM (Leshchinsky 2013; Leshchinsky and Ambauen 2015), while comparisons with FEM have been focused on bearing capacity problems (Gourvenec and Mana 2011; Leshchinsky 2015; Smith and Tatari 2016; Zheng et al. 2019; Zhou et al. 2018a; Zhou et al. 2018b). It is, therefore, appealing to not only investigate the performance of a simplified NGI-ADP model in DLO, but also to verify the results against both FEM and LEM.

Geometry and parameter variations

An idealised slope was chosen to investigate the performance, with slope inclination $\alpha = [15°, 90°]$ with 15° increments and H=10 m in Figure 7.1. The anisotropic shear strength was applied as (i) an increase of s_u^A; (ii) a decrease of s_u^P and (iii) a combination of both, in addition to an isotropic reference case, see Table 7.1. For instance, the abbreviation AP1.4 reads as $s_u^A = 1.4 s_u^{DSS}$ and $s_u^P = 0.6 s_u^{DSS}$.
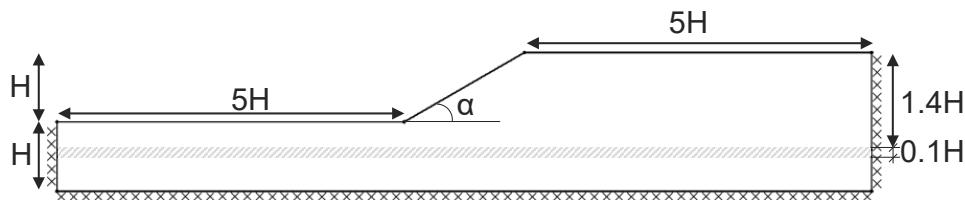

Figure 7.1: *Dimensions and boundary conditions with an optional weak layer highlighted. From Paper B.*

Table 7.1: *Applied shear strengths. From Paper B.*

Definition	Abbreviation	Values of n
Isotropic	I	1
s_u^A / s_u^{DSS}	An	1.1, 1.2, 1.3, 1.4, 1.5
s_u^P / s_u^{DSS}	Pn	0.5, 0.6, 0.7, 0.8, 0.9
s_u^A / s_u^{DSS} and $2 - s_u^P / s_u^{DSS}$	APn	1.1, 1.2, 1.3, 1.4, 1.5

Additionally, three soil types were applied, presented in Table 7.2. Further description of preconditions and nodal densities are found in Paper B.

Table 7.2: *Definition and abbreviation of applied soil types.*

Homogeneous soil	Constant s_u^{DSS}
Homogeneous soil, inc. su	Linearly increasing s_u^{DSS} with level
Heterogeneous soil, inc. su	Linearly increasing s_u^{DSS} with level, with isotropic weak layer $0.1 s_u^{DSS}$

Comparison with LEM and FEM

The methods were compared with respect to failure mode and the relative change of the safety factor:

$$\Delta F = \frac{F_{DLO} - F_{other}}{F_{other}} \tag{7.1}$$

applied with F_{LEM} and F_{FEM} respectively. The results show a good agreement in safety factor between DLO and FEM, with the anisotropic DLO deviating 5-8% from the numerical implementation in FEM, as summarised in Figure 7.2a. Generally, DLO results in a safety factor equal to or higher than the reference value from FEM for $15° \leq \alpha \leq 75°$, when the failure mode is non-restricted. For slope angles $>75°$, however, DLO consistently results in a lower safety factor than FEM with less than 5 percentage points deviation. The corresponding results for isotropic conditions, as illustrated as stars in Figure 7.2b, show the same magnitude of deviations. This illustrates that the anisotropic implementation in DLO does not necessarily result in larger deviations than the deviations inherited from the methods themselves.

The obtained magnitude of the deviations affects the second decimal in the safety factor for the range of F=1.0-1.99. This is likely an acceptable deviation for practical purposes, given the other uncertainties in a slope stability assessment highlighted in chapter 5. For instance, the uncertainty of the undrained shear strength alone is minimum 10% (Phoon and Kulhawy 1999). Additional comparisons between DLO and the conventional LEM in Figure 7.2, highlight the built-in uncertainties in LEM when both failure mechanisms and anisotropic functions are, in the best case, empirically assigned by the user.
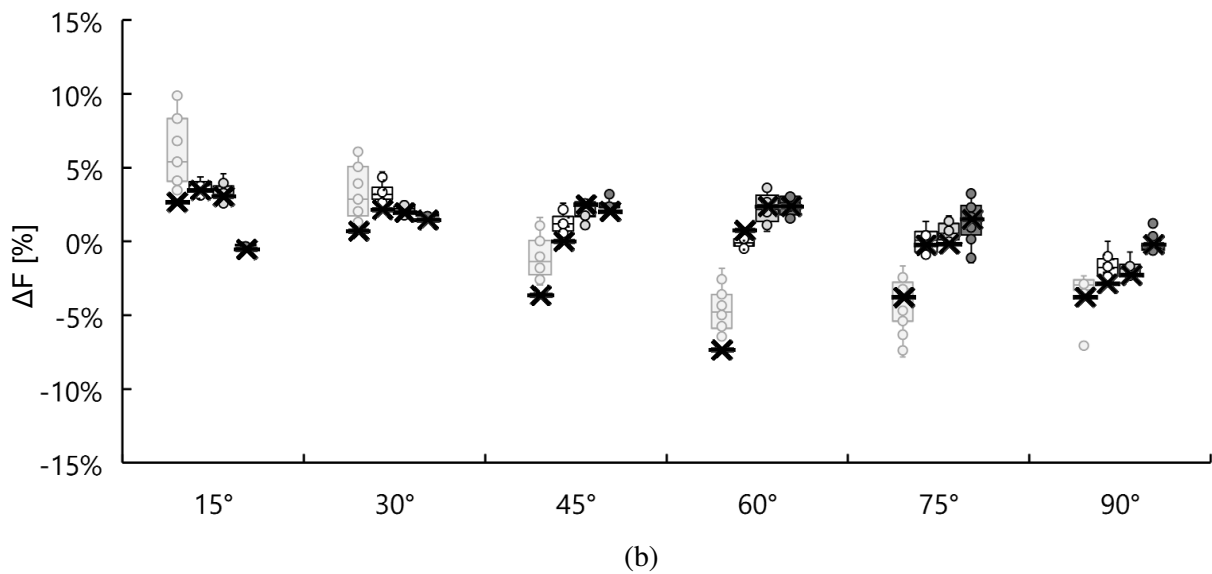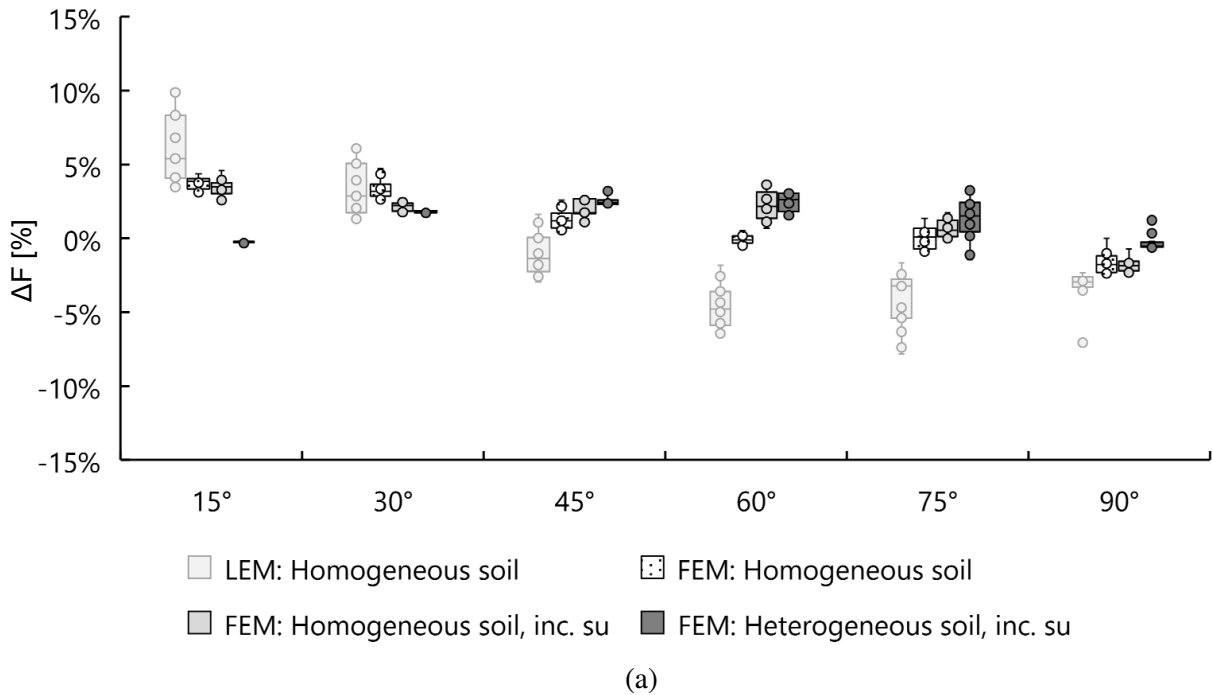
Figure 7.2: *Summary of relative change of safety factor with slope inclination for (a) anisotropic combinations with (b) isotropic results overlayed.*

Figure 7.3 and Figure 7.4 show how the failure modes from LEM (grey volumes) and FEM (black-white gradient) are captured by DLO (solid lines), respectively. The failure modes from FEM for heterogeneous soil show an inconclusive shear band on the active side, which was obtained from DLO by the use of internal (rotational) boundaries, see description in Paper B-Appendix C. The three internal boundaries; vertical from slope toe, vertical from slope crest and parallel with slope inclination, are seen as black lines in Figure 7.4. It is also evident for the 75° slope that an internal boundary needs to be sufficiently close to the collapsing area to affect the width of the failure mode.
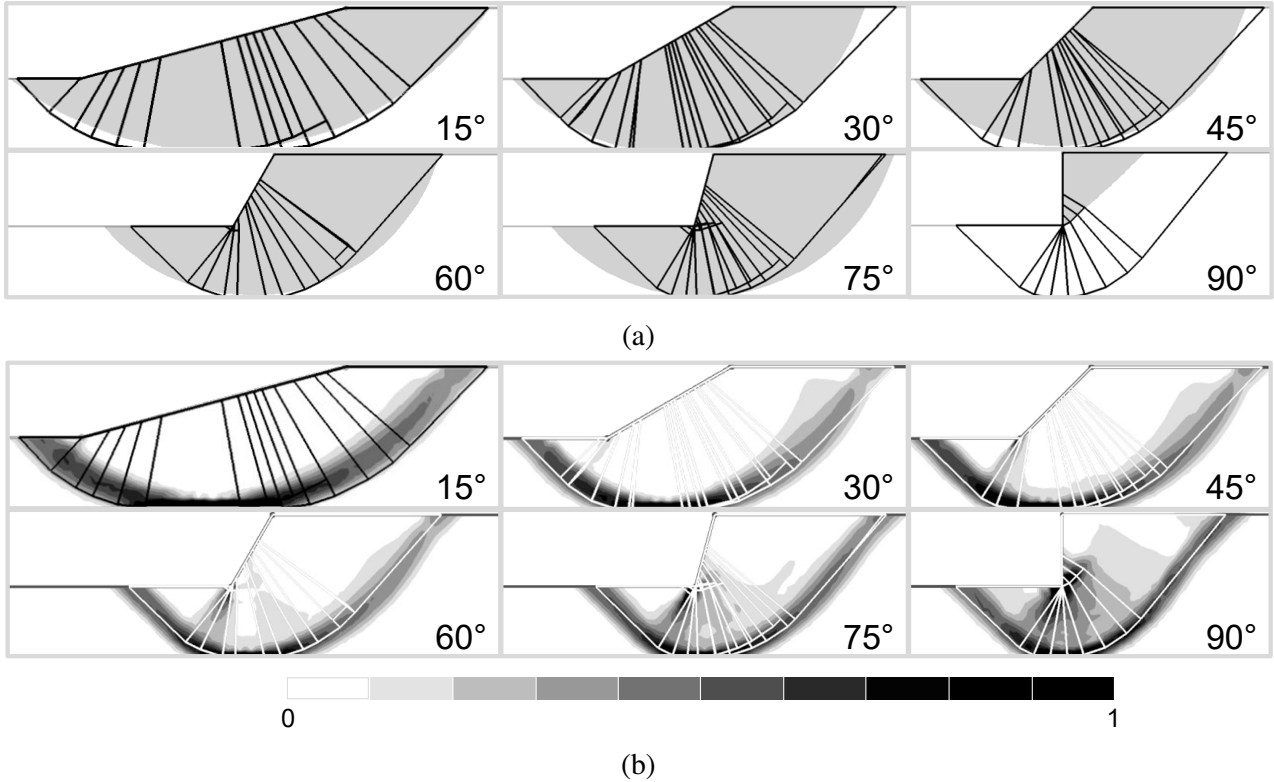
(a)

(b)

Figure 7.3: *Comparison of failure modes for homogeneous soil with AP1.5, with solid lines representing the individual blocks obtained using DLO; (a) against LEM, here represented as grey volumes, and (b) against the normalised incremental deviatoric strain ($\Delta\gamma_s/\Delta\gamma_{s,max}$) from FEM.*
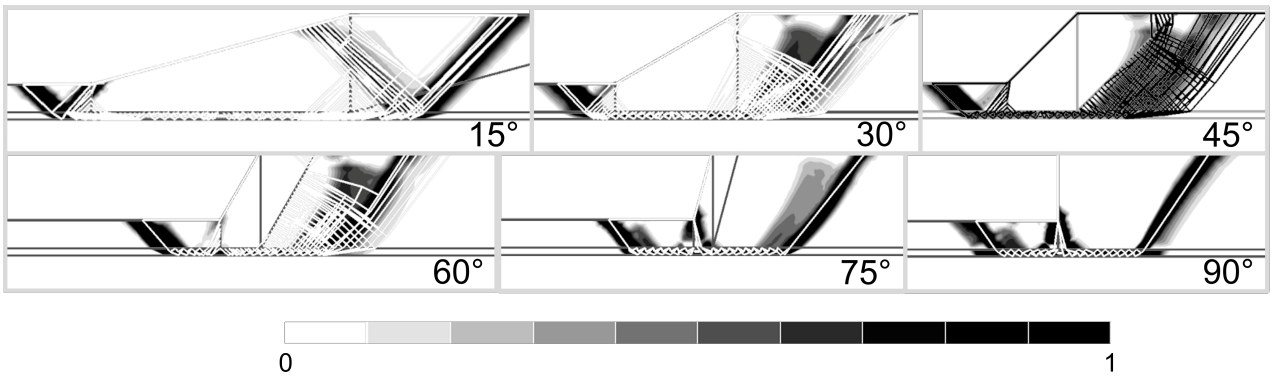

Figure 7.4: *Failure modes for heterogeneous soil with AP1.5. Solid lines are results from DLO and black-white gradients are the normalised incremental deviatoric strain ($\Delta\gamma_s/\Delta\gamma_{s,max}$) from FEM.*

Applicability

The results show that DLO is indeed capable of including total stress anisotropy in a rigorous manner and is thus an attractive supplement to LEM and FEM. The slip-line based discretisation circumvents the problems with numerical convergence that occurs in FE-based methods, and is at the same time accessible with straightforward input parameters and low computational times.

7.2 Creep-SCLAY1S in slope stability

Rate-dependency in slope stability assessment can be divided into three categories defined by Terzaghi (1950) for slope movement: (i) displacements due to external factors, (ii) seasonal creep along an existing slip surface and (iii) continuous creep in the whole soil mass, where the latter two can be triggered by external and micro-mechanical changes.

A literature review of previous research in the three categories is found in Paper C, but methods for simulating continuous creep in the whole soil mass for sensitive clays are very rare. For instance, the viscoplastic model presented by Hinchberger and Rowe (2005) does not account for anisotropic or strain-softening response, while Zhou et al. (2005) includes both features but applied in embankment (loading) type of problem. Both soil models are based on Perzyna's overstress theory (Perzyna 1963), with the key assumption of a pure elastic region, which contradicts experimental observations (Yin et al. 2011) and thereby also makes model calibration cumbersome, in contrast to Creep-SCLAY1S.

Previous studies using Creep-SCLAY1S include man-made embankments (Amavasai et al. 2018; Hernvall et al. 2021), which showed good agreement with field observations, and excavations supported with sheet-pile walls (Tornborg et al. 2023; Tornborg et al. 2021). In the latter, the soil model could successfully capture both the displacements and pore pressures during and after excavation. The unloading problem exhibited in a natural slope is, however, a different type of unloading problem, since the initial stress state (and state of the soil) in a natural slope is often unknown.

Given the formulation of Creep-SCLAY1S, with a mobilised strength dependent on state parameters, and no designated strength parameters, the failure is determined using an increase of the gravity in the model, similar to a centrifuge test. The methodology described in the following sections refers to the FE software PLAXIS 2D and its in-house implementation of Creep-SCLAY1S. Additionally, comparative simulations have been performed with the FE software COMSOL Multiphysics (Karlsson et al. 2021).

Initialisation of stresses

A FE simulation using Creep-SCLAY1S should start with a horizontal ground surface and horizontal soil layers, given the mathematical assumptions on the initial anisotropy, i.e. the components of the deviatoric fabric tensor using α_0. For the case of natural slopes, the soil parameters should be calibrated against soil samples taken from horizontal ground corresponding to the level at slope crest. In that way, the risk of uncertainties due to built-in stress rotations in the soil samples, due to unloading in the slope area, is reduced.

Figure 7.5 shows an example of validation of the chosen state parameters in Paper C for the benchmark slope against field- and laboratory tests taken from the site. Here, the slope geometry was initiated with horizontal ground surface and 10 years of consolidation, followed by an extraction of 6 FE element clusters from one cross section at various depths. A Direct Simple Shear (DSS) simulation was then performed on each element, with the predicted peak strength presented in the graph. The results show very good agreement between the measured undrained shear strength on site and the corresponding predicted values from Creep-SCLAY1S.
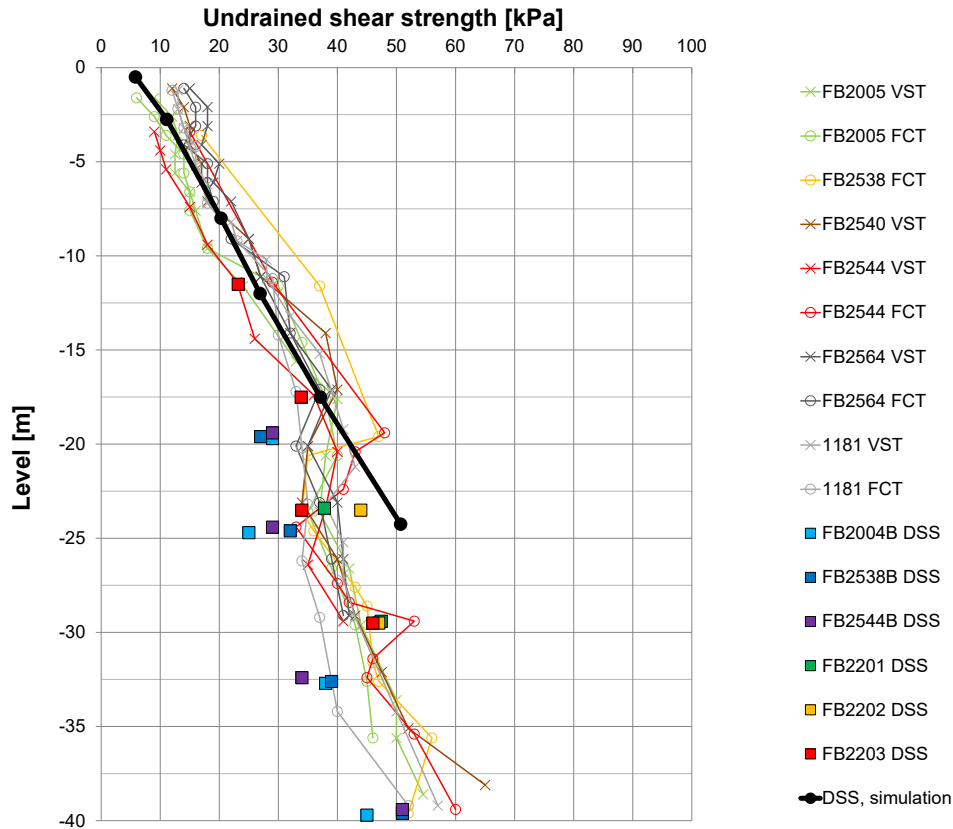
Figure 7.5: *Uncorrected vane shear tests (VST), uncorrected fall cone tests (FCT) and direct simple shear tests (DSS) taken from the site. Black points are simulated DSS tests of elements extracted from the FE model after consolidation of horizontal ground surface.*

The following calculation steps include any historical natural/man-made alterations of the ground surface, and changes in pore pressures, to simulate the geological processes that resulted in the current geometry of the slope. Figure 7.6 illustrates such simplified simulation of the geological process adopted in the simulation.
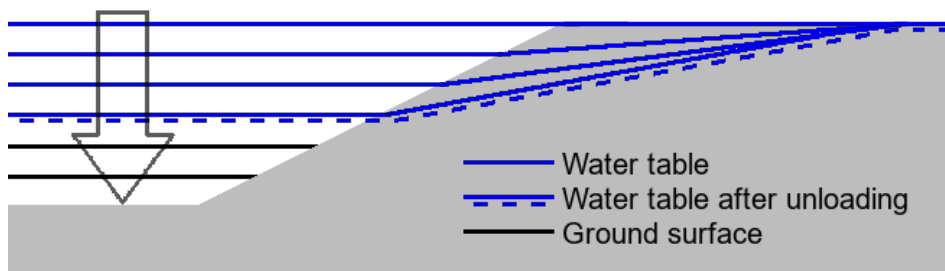

Figure 7.6: *Calculation phases from horizontal ground surface and ground water level up to the final geometry and pore pressure distribution. From Paper D.*

Ideally, each surface- or pore pressure alteration should be assigned the actual time, to include any creep deformations. This is however non-trivial or perhaps even impossible for natural slopes, as the soil sampling for parameter calibration then should have been performed at time zero in

the FE simulation. Additionally, the original levels and the geometric and geological changes are seldom known. For the benchmark slope simulations in Paper C-D, each calculation phase was assigned sufficient time to let (negative) excess pore pressures dissipate, and yet still have a final slope geometry corresponding to the slope geometry on site.

Safety analysis

The stability of the slope can be investigated by an increase of gravity until failure occurs, similar to a centrifuge test. The default application time of the increased gravity is set to 24 h in Paper C-D, to represent an undrained response (high loading rate) and at the same time correspond to the reference time given for Creep-SCLAY1S. The concept of reference time is further explained in section 3.4. Such short time span is also favourable to avoid any consolidation effects during the safety analysis. In PLAXIS, the user assigns a target gravity, ΣM_{weight}, which is scaled by a multiplier, ΣM_{stage}, ranging from 0 to 1, resulting in an applied gravity in each calculation step as:

$$\Sigma M_{gravity} = 1 + \left[\Sigma M_{stage} \cdot (\Sigma M_{weight} - 1) \right] \tag{7.2}$$

where the first term represents the inherited gravity and stress history from the initialisation, and the second term represents the additional gravity added during safety analysis. For the following used reference case, with ΣM_{weight}=2-g, the expression can be simplified to:

$$\Sigma M_{gravity} = 1 + \Sigma M_{stage} \tag{7.3}$$

Given the implementation in PLAXIS, this means a linear relationship between time and applied gravity, illustrated in Figure 7.7. Here, the dots represent the calculation increments obtained from the software.
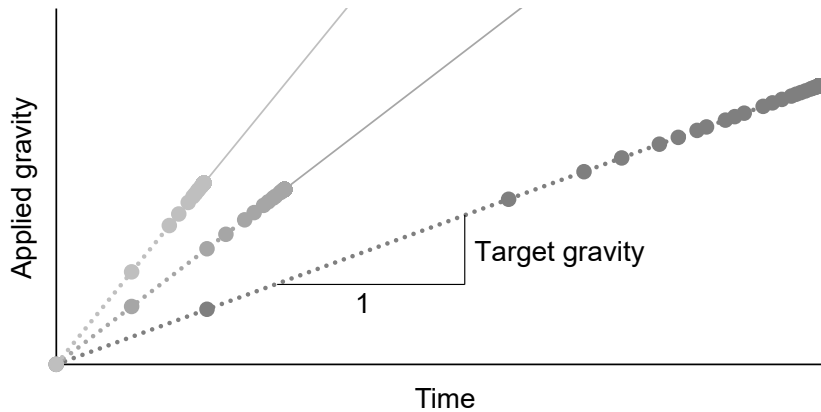

Figure 7.7: *Effect of varying target gravity on applied gravity with the same application time.*

By using a relatively short application time for ramping the gravity, a sufficiently large value of ΣM_{weight} will generate an excess pore pressure to the extent that a shear band will form and large displacements will develop. As previously discussed, in FE safety analysis, the calculation will end up at a constant value of ΣM_{stage} when the model reaches non-convergence. This is seen e.g. in Figure 7.7 where the applied gravity increments reduce until infinitely-small.

Figures 7.8 to 7.11 show examples of the results from the reference simulation in Paper C of the benchmark slope. Here, Figure 7.8 highlights how the stresses rotate by the unloading (left) and by the increased gravity (right). Figure 7.9 shows that the fabric tensor components respond to the emerging strains. Figure 7.11 presents the failure surface and the effective stress paths in three points along the shear band. All three figures demonstrate how the stress state and state of the soil (anisotropy) is evolving, and how the failure is initiated at the slope toe. A detailed description of the safety analysis is found in Paper C.

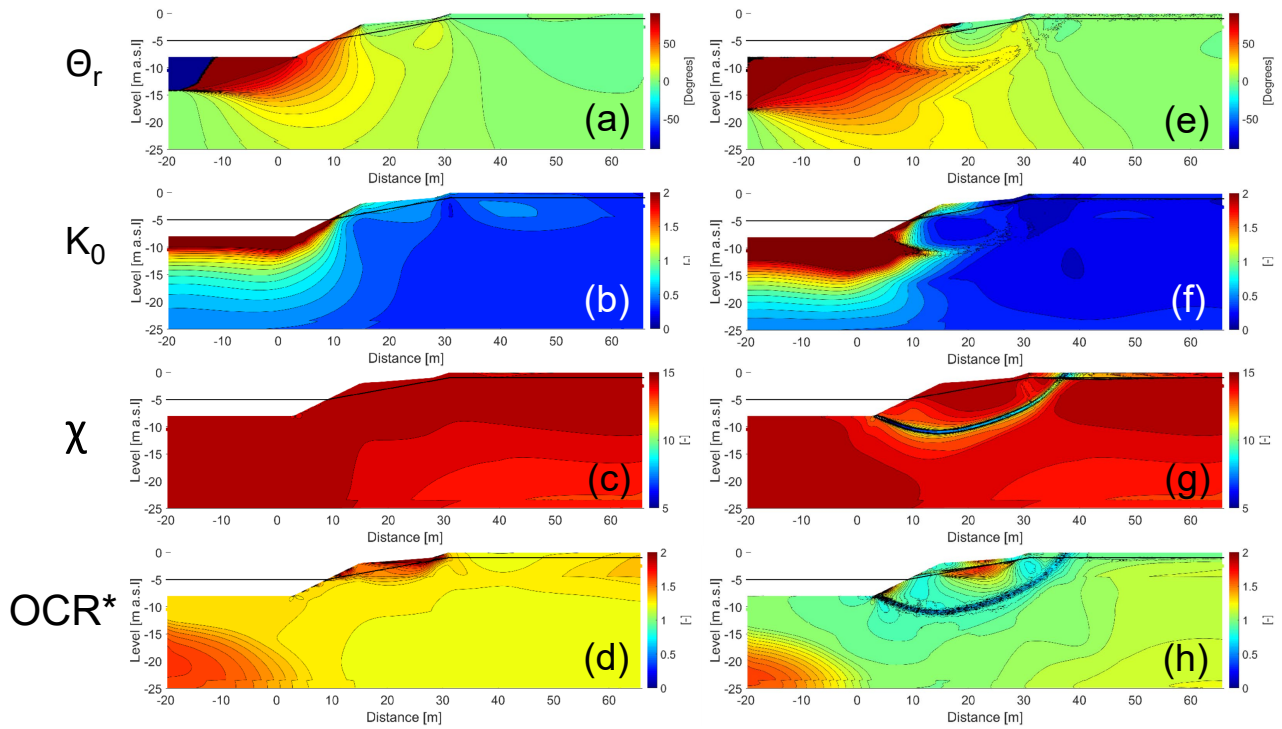Figure 7.8: *Contour plots of principal stress direction, θ_r (upper row), K_0 (second row), the amount of bonding, χ (third row) and OCR* (lower row) after unloading (left) and after additional gravity is applied (right). Modified from Paper C.*
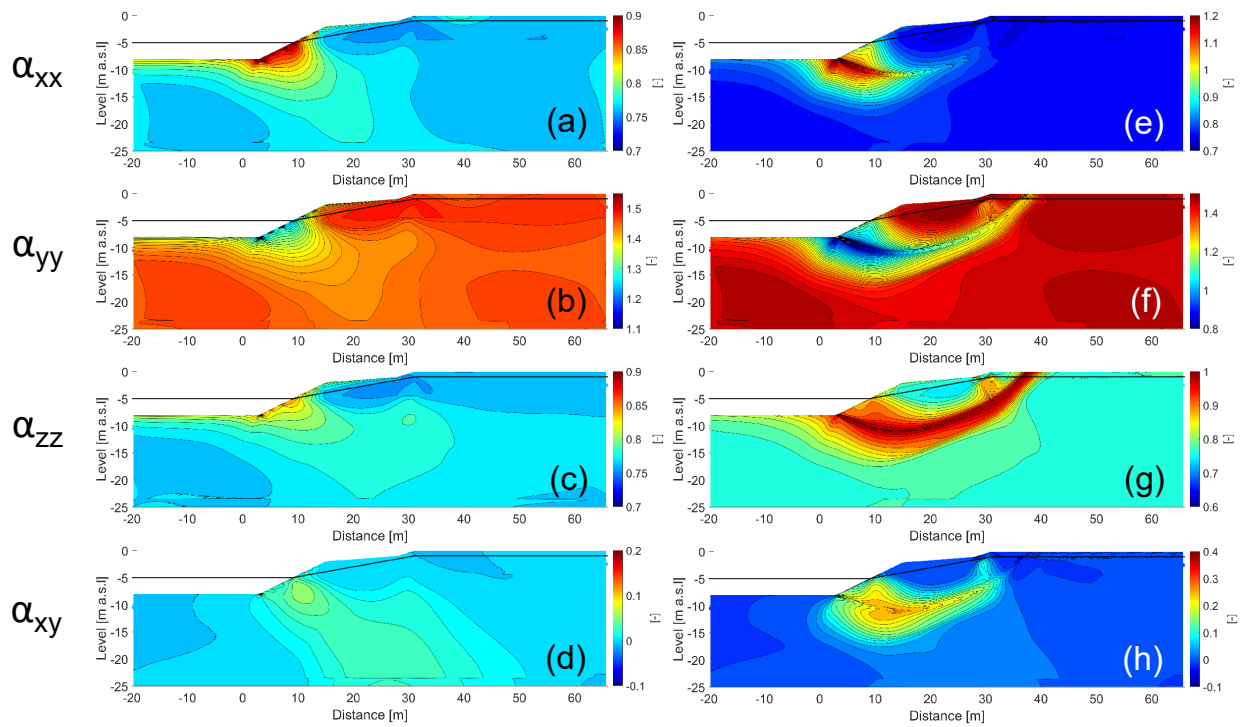
Figure 7.9: *Fabric tensor components after unloading (left) and after additional gravity is applied (right). Modified from Paper C.*

Figure 7.10: *Location of chosen elements in the shear band. Modified from Paper C.*

(a)   (b)   (c)

Figure 7.11: *Effective stress paths for the elements in Figure 7.10 for general stress space. 'X' marks the initial stress before unloading and red circle marks where gravity is increased above 1. Modified from Paper C.*

Applied gravity

The obtained gravity at failure, to be considered as a proxy to the safety factor, is dependent on the assigned target gravity, and the resulting application rate. The applica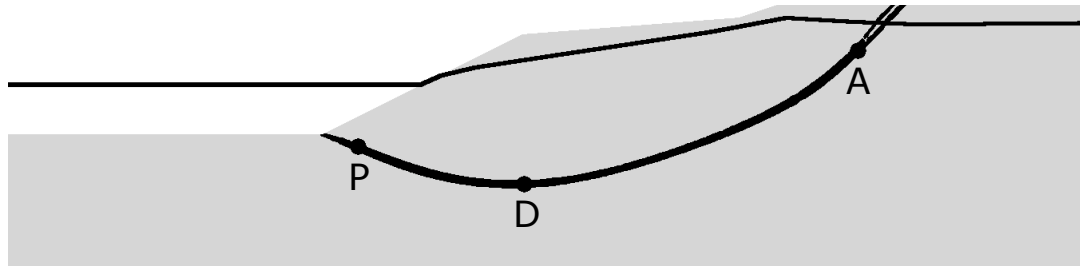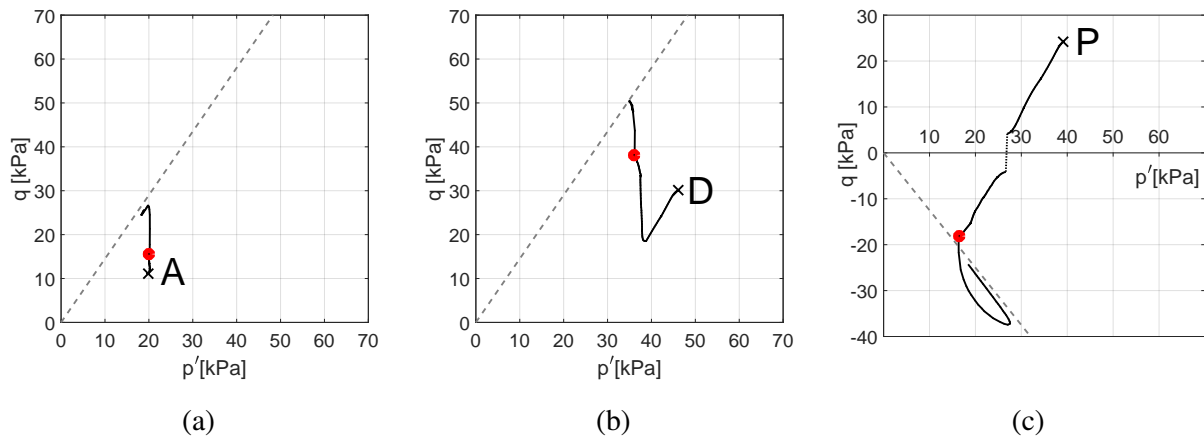tion rate governs the excess pore pressure generation, and relatively long application times will also result in some unrealistic creep effects and subsequent deformations.

The benchmark slope is here used to illustrate the effect of varying the target gravity, ΣM_{weight}, with a constant application time equal to τ_{ref}. This means that an increase of the target gravity in this case will result in an increase of the rate of gravity. Figure 7.12 shows how the gravity at failure, $\Sigma M_{gravity}$, is almost constant after a threshold value, just as the total horizontal displacements at slope toe. It is evident that the applied rate of gravity ($\Sigma M_{weight}/\tau_{ref}$) mainly affects the time to reach a triggering excess pore pressure level, and only have a minor influence on the obtained gravity at failure. The corresponding failure mode is also almost identical, as shown in Figure 7.13 for the extreme cases ΣM_{weight}=1.7 and 5.0.
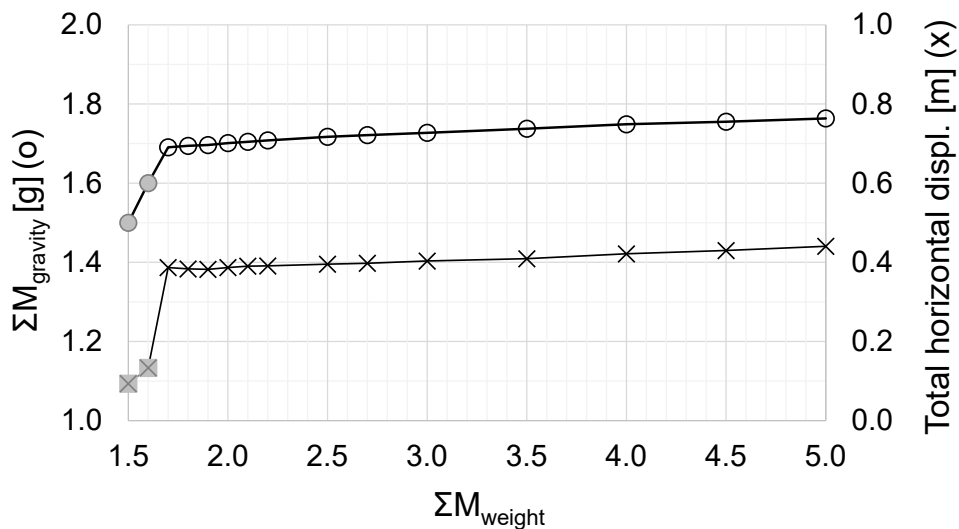

Figure 7.12: *Results from 15 different target gravities with 24 h application time, respectively. Highlighted marks did not reach failure within the given time. Displacements refers to point Q in Figure 7.13. Modified from Paper C.*
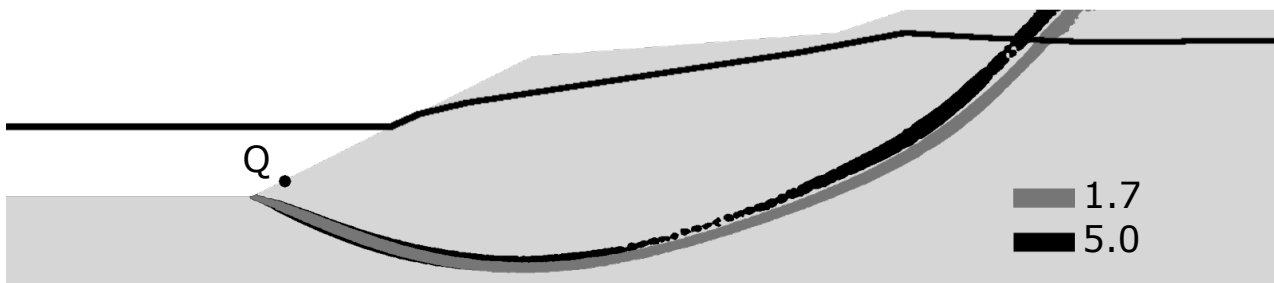

Figure 7.13: *Failure surface using two different ΣM_{weight} with 24 h application time.*

Figure 7.14 shows the excess pore pressures in points A, D, and P from Figure 7.12 for all 15 safety calculations. Here, ΣM_{stage} on the x-axis shows how much additional gravity needed to be applied to reach failure, given the different loading rates. For the cases $\Sigma M_{weight} = 1.5 - 1.6$ with black dashed/dotted lines, the excess pore pressures are indeed increasing in all three points, but never accelerate and thus confirm that no failure occurs. For $\Sigma M_{weight} = 1.7$, the excess pore pressure in point P is gradually increasing until an initial soil collapse, followed by a force re-distribution along the shear band which results in an acceleration of excess pore pressures in point A and D within the shear band. Additionally, Figure 7.14 shows a small change in magnitude of excess pore pressure in point P when $\Sigma M_{weight} = 5.0$ compared to $\Sigma M_{weight} = 1.7$. This difference could be the reason for the slightly smaller slip surface for $\Sigma M_{weight} = 5.0$ in Figure 7.13. In general, the total area of the slip surfaces between $\Sigma M_{weight} = 1.7 - 5.0$ is slightly shrinking from the shape at $\Sigma M_{weight} = 1.7$ as ΣM_{weight}, and thereby the loading rate, increases.

The total horizontal displacements discussed here are indicative for the values for small or large movements, and not actual horizontal movements during a failure. These values, and the results in Figures 7.12 to 7.14 are also sensitive to the number of elements in the model and the mesh density. Just as with any FE analysis, the user needs to verify that the results are independent of the mesh. In the case of FE safety analysis, a finer mesh results in a thinner shear band, but could lead to other unexpected results. For instance, the horizontal movements at slope toe in the benchmark slope varied up to 55% with the mesh density (Paper C).

It should also be noted that the safety analyses performed with increased gravity in PLAXIS (version 21.01.00.479) do not apply the increased gravity equally to the weight of soil and water. The soil weight is increased incrementally, as expected:

$$\gamma_{soil,i} = \Sigma M_{gravity,i} \cdot \gamma_{soil,start} \quad \text{where } 1 \leq \Sigma M_{gravity,i} \leq M_{weight} \tag{7.4}$$

whereas the weight of water is assigned its final value in the first calculation step:

$$\gamma_{water,i} = \Sigma M_{gravity} \cdot \gamma_{water,start} \quad \text{where } \Sigma M_{gravity} = \Sigma M_{weight} \tag{7.5}$$

This error can be reduced by manual iterations of ΣM_{weight} to obtain a value that approaches failure.
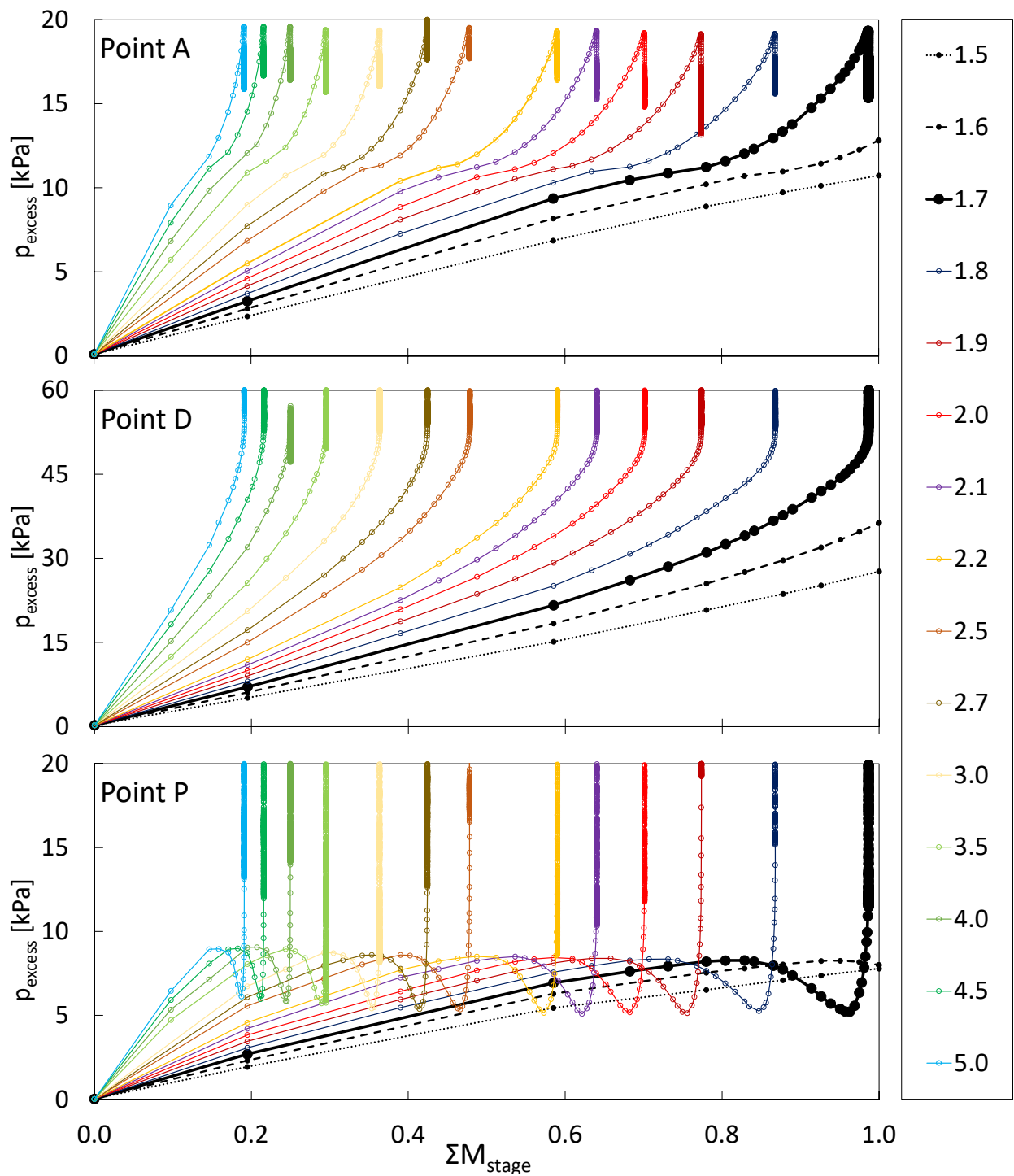
Figure 7.14: *Excess pore pressures in point A, D, P from Figure 7.13 during 15 safety calculations with different ΣM_{weight} and 24 h application time. See also Figure 7.12.*

Comments on rate-dependency

The proposed method includes two rate-dependent components; the soil model and the application rate of gravity in terms of $\Sigma M_{gravity}$. However, by having that, the obtained failure mode consists of a combination of excess pore pressures (the rate of gravitational increase) and the creep rate (the soil model response together with the application time). An example of this is found in Figure 7.15, where it cannot be separated whether the slip surface with long application time is shallow due to a drained failure or due to creep. Nevertheless, given the tendency of natural clays to creep, and the fact that the failure is triggered by changes in effective stress, the rate of change of any environmental effects that result in those effective stress changes will affect the resulting safety factor, as illustrated with the gravity at failure in Figure 7.15. Thus, one may question how appropriate it is to use the concept of a safety factor.
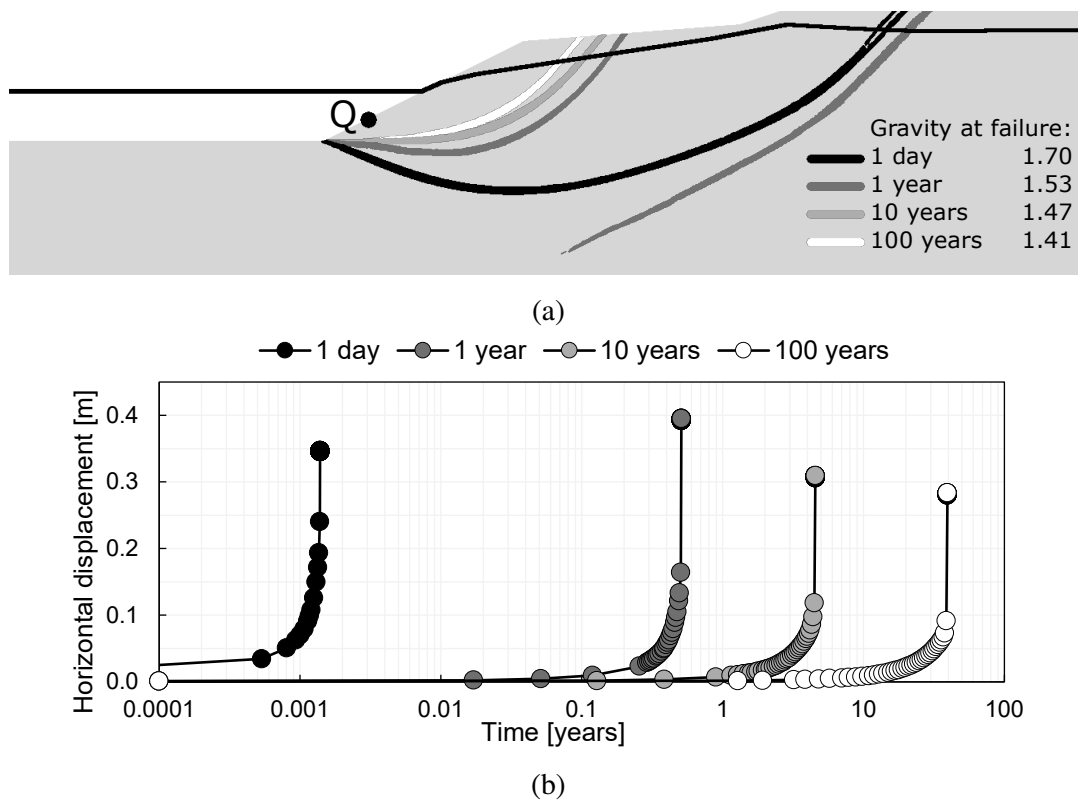
Figure 7.15: *(a) Failure surface from various applications time of increased gravity, all with a target gravity of 2. (b) Horizontal displacements in point Q during safety calculation. From Paper C.*

Influence of soil fabric and apparent structure

Given the hierarchical structure of Creep-SCLAY1S, the influence of soil fabric (initial and evolving anisotropy) and the apparent structure (the bonds acting between the clay particles and their destructuration) on slope stability can be investigated separately, see details in Paper D. To refer to the flowchart of a stability assessment in Figure 5.1, it is indeed interesting to investigate if all features in this complex soil model are necessary for this type of ULS problem.

For these simulations, a constant rate of gravity was set to 2-g/24 h, which means that $\Sigma M_{gravity}$ here has an upper limit of 2.0. It should be noted that the definition of the applied gravity in Paper D, referred to as ΣM_{total}, has an error which allow for applied gravities less than 1-g. All values presented herein are referring to $\Sigma M_{gravity}$ only. The two values are related as:

$$\Sigma M_{gravity} = 1 + \frac{\Sigma M_{total}}{2} \tag{7.6}$$

Figure 7.16 shows how the failure varies with both soil fabric and apparent structure. The fixed anisotropy in Figure 7.16c results in an underestimation of the mobilised shear strength at the slope toe, which results in a relatively low ΣM_{total} at failure and a shallow failure mode. Inclusion of the evolving anisotropy means that the simulations to the current initial state, due to unloading and dewatering, results in the anisotropy varies within the slope. This affects both failure mode and the ultimate gravity at failure.

The destructuration changes the failure mode for fixed anisotropy, Figure 7.16a and Figure 7.16c respectively, while the cases with evolving anisotropy, Figure 7.16b and Figure 7.16d, only result in different width of the shear band. The inclusion of destructuration in the simulations does however reduce the gravity at failure for both initial and evolving anisotropy, implying that the initial structure and the destructuration affect the progression of the failure.

(a) *Fixed anisotropy without structure, 1.43-g*   (b) *Evolving anisotropy without structure, 1.93-g*

(c) *Fixed anisotropy with structure, 1.33-g*   (d) *Evolving anisotropy with structure, 1.70-g*
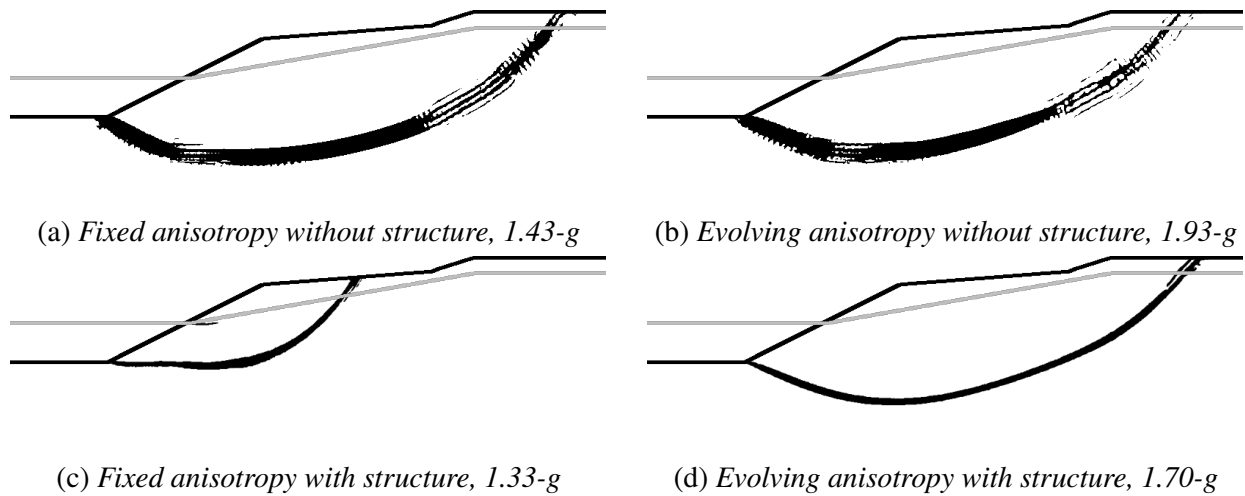
Figure 7.16: *Failure modes and gravities at failure, $\Sigma M_{gravity}$. Modified from Paper D.*

Overall, the results show that both evolving anisotropy and destructuration are of importance when simulating slope stability in sensitive soil using a rate-dependent model, in order to account for the spatially varying stress distribution and the corresponding soil response.

8   Conclusions and recommendations

The aim of this thesis was to incorporate new soil models and modelling techniques for the stability assessment of natural slopes in sensitive clays. An objective was to consider how to account for the evolving hydromechanical processes and the strength anisotropy, respectively. The motivation for the work is the need to develop new approaches for assessing slope stability, given many natural slopes are currently deemed unstable or critical, and yet the number of failures are relatively limited. Furthermore, with climate change, fluctuations in the pore pressure regime would be expected, requiring a coupled effective stress based analyses, even when only considering the fully saturated case.

The methodologies consisted of three parts of incremental complexity:

    i Comparison on various available methods for slope stability with a simple soil model.

    ii Verification of a user-adaptable total stress based anisotropic failure criterion for upper bound limit analysis of slope stability.

    iii Application of an advanced effective stress based soil model to capture the rate-dependent and spatially varying soil response.

Firstly, stability analyses of a slope with a simple soil model (Mohr-Coulomb failure criterion), highlighted that whilst all methods used (LEM, DLO, FELA and FEM) produced similar results for the undrained case, the same did not apply to the drained case. Furthermore, the simple model did not account for anisotropy of the undrained strength.

In order to study the effect of anisotropy, secondly as a straightforward extension, an user-defined undrained shear strength that is representative for the stress history and the stress rotations in the slope was adopted in DLO, compared with FE analyses with the NGI-ADP model. Additional comparison was done with LEM with the user-defined shear strength scale factor to emulate the yield criterion in the NGI-ADP model. The method showed good agreement in terms of safety factor and failure mode in the (total stress based) reference cases, with a reduced computational cost. This highlights the potential for advancement from conventional slope stability assessment in LEM, since no *a-priori* assumptions of the critical slip surface are needed. Yet, still anisotropy is included with a solid framework, verified against the NGI-ADP model, for the Ultimate Limit State.

In the third method, a novel approach is proposed to simulate the genesis of a natural slope up to its current state using an advanced soil model. In that manner, the user only assigns critical state parameters, while the evolving state variables during the simulated loading history control the magnitude and distribution of e.g. anisotropy, and thus the mobilised rate-dependent strength. The results showed that it is feasible to adopt a rate-dependent soil model for slope stability analyses. Successful use, however, requires great care into the model initialisation (effective stress and other state parameters). The best results were indeed obtained by simulating the geological formation in a simplified manner. This study also highlighted that undisturbed sampling from sloping ground surface, i.e. within a slope, will recover samples with built-in stress and fabric rotations that will affect the laboratory tests. Therefore, the estimated mobilised shear strength evaluated from element level tests on such samples taken from natural slopes do not necessarily represent the

in-situ strength.

Rate-dependent models implemented in a Finite Element code, as used in this thesis, require the gravity increase method for slope stability analyses. In this type of analyses, the rate of increasing the gravity (hence body forces in the domain) had a significant impact on the mobilised shear strength, thereby also the calculated stability. Furthermore, to some extent the failure mechanism triggered was also impacted by the rate of loading. High rates of loading, 1.7-g/24h and above, generated a typical undrained response, with the time to failure equal to the time to reach the magnitude of excess pore pressure required to develop a continuous shear band. The failure of a slope (and the safety factor) thus depends on the rate of environmental (pore pressure) change.

In addition, a numerical study on the influence of fabric orientation and bond degradation on the failure mode was conducted. The results showed that at a constant loading rate, all features in the model affect the development of excess pore pressures, and thereby the reached level of gravity at failure. The bond degradation was also shown to affect the progression of the failure mechanism. Thus, when studying the potential for slope failure in a sensitive clay slope, it is necessary to incorporate all model features (rate effects, anisotropy, bonding and bond degradation).

This thesis has highlighted the importance of the initial conditions in a slope, including complex stress rotations and anisotropy, for calculating the stability. Furthermore, the transient micro-mechanical changes, resulting with bond degradation and evolution of anisotropy, acting in a slope that are driven by groundwater flow were studied. The coupled flow-deformation analyses enable to understand the consequences of a changing climate in natural slopes in sensitive clay, and enable to account for different patterns of precipitation, time-dependent pore pressure changes and erosion. The work has also shown that simplifications are necessary for practical applications, as well as that the use of a safety factor alone as a measurement of global stability can be misleading.

There is still a need to find the right level of complexity of soil model and safety analysis, in order to capture the soil response in a natural slope, ultimately to reach a consistent and accessible quantification of the effect of climate change on slope stability.

Suggestions for further studies are thereby:

i Verify the use of Creep-SCLAY1S in a full-scale cut slope, from undisturbed sampling at horizontal ground surface, via documented excavation steps with monitored pore pressure changes, up to slope failure.

ii While the use of a rate-dependent model was successful for initialisation of the effective stresses and spatially varying state of the natural clay, there were, however, some concerns in the safety analysis with respect to the safety factor. The application of an improved safety analysis should be further investigated, e.g. by freezing the state parameters (and thus hardening) during the phase of the safety analysis.

iii Finally, given the uncertainties in soil and state parameters, as well as the hydrogeological conditions, it would be advisable to explore the idea of replacing the safety factor with a safety interval, using soil properties for a lower bound worst scenario and an upper bound cautious estimate, as suggested by Fellin (2005).

References

Amavasai, A., Sivasithamparam, N., Dijkstra, J., & Karstunen, M. (2018). Consistent Class A & C predictions of the Ballina test embankment. *Computers and Geotechnics*, *93*, 75–86.

Birmpilis, G., Andò, E., Stamati, O., Hall, S. A., Gerolymatou, H. E., & Dijkstra, J. (2022). Experimental quantification of 3D deformations in sensitive clay during stress-probing. *Géotechnique*, (Advance online publication), 1–12.

Bishop, A. W. (1955). The use of the slip circle in the stability analysis of slopes. *Géotechnique*, *5*(1), 7–17.

Bjerrum, L. (1973). Problems of soil mechanics and construction on soft clays and structurally unstable soils-collapsible expansive and others. State-of-the-art report to session IV. *8th International Conference on Soil Mechanics and Foundation Engineering*, 111–159.

Brinkgreve, R. B. J., & Bakker, H. L. (1991). Non-linear finite element analysis of safety factors. *Proc. 7th Int. Conf. on Comp. Methods and Advances in Geomechanics, Cairns, Australia*, 1117–1122.

Burland, J. B. (1990). On the compressibility and shear strength of natural clays. *Géotechnique*, *40*(3), 329–378.

Casagrande, A., & Wilson, S. D. (1951). Effect of rate of loading on the strength of clays and shales at constant water content. *Géotechnique*, *2*(3), 251–263.

Chen, W. F., & Mizuno, E. (1990). *Nonlinear analysis in soil mechanics*. Elsevier.

Christian, B. J. T., Ladd, C. C., & Baecher, G. B. (1994). Reliability applied to slope stability analysis. *Journal of Geotechnical Engineering*, *120*(12), 2180–2207.

Comegna, L., Picarelli, L., Bucchignani, E., & Mercogliano, P. (2013). Potential effects of incoming climate changes on the behaviour of slow active landslides in clay. *Landslides*, *10*(4), 373–391.

Crosta, G. B., Frattini, P., Castellanza, R., Frigerio, G., di Prisco, C., Volpi, G., De Caro, M., Cancelli, P., Tamburini, A., Alberto, W., & Bertolo, D. (2015). Investigation, monitoring and modelling of a rapidly evolving rockslide: The Mt. de la Saxe case study. In G. Lollino, D. Giordan, G. B. Crosta, J. Corominas, R. Azzam, J. Wasowski, & N. Sciarra (Eds.), *Engineering Geology for Society and Territory - Volume 2* (pp. 349–354). Springer International Publishing.

Davis, E. H., & Christian, J. T. (1971). Bearing capacity of anisotropic cohesive soil. *Journal of the Soil Mechanics and Foundations Division*, *97*(5), 753–769.

Delage, P., & Lefebvre, G. (1984). Study of the structure of a sensitive Champlain clay and of its evolution during consolidation. *Canadian Geotechnical Journal*, *21*(1), 21–35.

Desai, C. S., Samtani, N. C., & Vulliet, L. (1995). Constitutive modeling and analysis of creeping slopes. *Journal of Geotechnical Engineering*, *121*(1), 43–56.

D'Ignazio, M., Länsivaara, T. T., & Jostad, H. P. (2017). Failure in anisotropic sensitive clays: Finite element study of Perniö failure test. *Canadian Geotechnical Journal*, *54*(7), 1013–1033.

Duncan, J. M., & Wright, S. G. (1980). The accuracy of equilibrium methods of slope stability analysis. *Engineering geology*, *16*(1), 5–17.

Eden, W. J. (1977). Evidence of creep in steep natural slopes of Champlain Sea clay. *Canadian Geotechnical Journal*, *14*(4), 620–627.

Emery, J. J. (1978). Chapter 19 - Simulation of slope creep. In B. Voight (Ed.), *Developments in Geotechnical Engineering: Rockslides and Avalanches, 1* (pp. 669–691). Elsevier.

Fellin, W. (2005). Ambiguity of safety definition in geotechnical models. In W. Fellin, H. Lessmann, M. Oberguggenberger, & R. Vieider (Eds.), *Analyzing Uncertainty in Civil Engineering* (pp. 17–31). Springer Berlin Heidelberg.

Fenton, G. A., & Griffiths, D. V. (2008). *Risk assessment in geotechnical engineering*.

Frank, R., Bauduin, C., Driscoll, R., Kavvadas, M., Ovesen, N. K., Orr, T., Schuppener, B., & Gulvanessian, H. (2015). *Chapter 11. Overall stability* (H. Gulvanessian, Ed.). Thomas Telford Publishing.

Geertsema, M., Menounos, B., Bullard, G., Carrivick, J. L., Clague, J. J., Dai, C., Donati, D., Ekstrom, G., Jackson, J., Lynett, P., Pichierri, M., Pon, A., Shugar, D., Stead, D., Del Bel Belluz, J., Friele, P., Giesbrecht, I., Heathfield, D., Millard, T., … Sharp, M. (2022). The 28 November 2020 landslide, tsunami, and outburst flood – A hazard cascade associated with rapid deglaciation at Elliot Creek, British Columbia, Canada. *Geophysical Research Letters*, *49*, 1–12.

Gens, A., & Nova, R. (1993). Conceptual bases for a constitutive model for bonded soils and weak rocks. In A. Anagnostopoulos (Ed.), *Prof. International Symposium on Hard Soils- Soft Rocks, 1993; Athens* (pp. 485–494). A A Balkema.

Gilbert, M., Smith, C. C., Haslam, I. W., & Pritchard, T. J. (2010). Application of discontinuity layout optimization to geotechnical limit analysis problems. In T. Benz & S. Nordal (Eds.), *Proceedings of the 7th European Conference on Numerical Methods in Geotechnical Engineering* (pp. 169–174). CRC Press.

Gourvenec, S. M., & Mana, D. S. K. (2011). Undrained vertical bearing capacity factors for shallow foundations. *Géotechnique Letters*, *1*(4), 101–108.

Graham, J., Crooks, J. H., & Bell, A. L. (1983a). Time effects on the stress-strain behaviour of natural soft clays. *Géotechnique*, *33*(3), 327–340.

Graham, J., Noonan, M. L., & Lew, K. V. (1983b). Yield states and stress-strain relationships in a natural plastic clay. *Canadian Geotechnical Journal*, *20*(3), 502–516.

Gras, J.-P., Sivasithamparam, N., Karstunen, M., & Dijkstra, J. (2017). Strategy for consistent model parameter calibration for soft soils using multi-objective optimisation. *Computers and Geotechnics*, *90*, 164–175.

Gras, J.-P., Sivasithamparam, N., Karstunen, M., & Dijkstra, J. (2018). Permissible range of model parameters for natural fine-grained materials. *Acta Geotechnica*, *13*(2), 387–398.

Grimstad, G., Andresen, L., & Jostad, H. P. (2012). NGI-ADP: Anisotropic shear strength model for clay. *International Journal for Numerical and Analytical Methods in Geomechanics*, *36*(4), 483–497.

Grimstad, G., Degago, S. A., Nordal, S., & Karstunen, M. (2010). Modeling creep and rate effects in structured anisotropic soft clays. *Acta Geotechnica*, *5*(1), 69–81.

Guzzetti, F. (2000). Landslide fatalities and the evaluation of landslide risk in Italy. *Engineering Geology*, *58*(2), 89–107.

Hernvall, H., Karlsson, M., Dijkstra, J., & Karstunen, M. (2021). Evolution of undrained strength under a test embankment. In M. Barla, A. Di Donna, & D. Sterpi (Eds.), *Challenges and Innovations in Geomechanics* (pp. 707–714). Springer International Publishing.

Hinchberger, S. D., & Rowe, R. K. (2005). Evaluation of the predictive ability of two elastic-viscoplastic constitutive models. *Canadian Geotechnical Journal*, *42*(6), 1675–1694.

Hu, C.-m., Yuan, Y.-l., Mei, Y., Wang, X.-y., & Liu, Z. (2019). Modification of the gravity increase method in slope stability analysis. *Bulletin of Engineering Geology and the Environment*, *78*(6), 4241–4252.

Hultin, S. (1916). Grusfyllningar för kajbyggnader. *Teknisk Tidskrift*, *V.U.h*(31), 292–294.

IPCC. (2021). Summary for Policymakers. In V. Masson-Delmotte, P. Zhai, A. Pirani, S. L. Connors, C. Péan, S. Berger, N. Caud, Y. Chen, L. Goldfarb, I. Gomis, M. Huang, E. Leitzell, E. Lonnoy, J. B. R. Matthews, T. K. Maycock, T. Waterfield, O. Yelekçi, R. Yu, & B. Zhou (Eds.), *Climate Change 2021: The Physical Science Basis. Contribution of Working Group I to the Sixth Assessment Report of the Intergovernmental Panel on Climate Change*. In Press.

Jaky, J. (1948). Pressure in silos. *Proceedings of the 2nd international conference on soil mechanics and foundation engineering*, 103–107.

Janbu, N. (1954). Application of composite slip surfaces for stability analysis. *Proceedings of the European Conference on Stability of Earth Slopes*, 43–49.

Jostad, H. P., Fornes, P., & Thakur, V. (2014). Effect of strain-softening in design of fills on gently inclined areas with soft sensitive clays. In J.-S. L'Heureux, A. Locat, S. Leroueil, D. Demers, & J. Locat (Eds.), *Landslides in Sensitive Clays: From Geosciences to Risk Management* (pp. 305–316). Springer Netherlands.

Karlsson, M., & Karstunen, M. (2017). On the benefits of incorporating anisotropy in stability analyses in sensitive clays. In V. Thakur, J.-S. L'Heureux, & A. Locat (Eds.), *Landslides in Sensitive Clays: From Research to Implementation* (pp. 259–266). Springer International Publishing.

Karlsson, M., Sellin, C., & Karstunen, M. (2021). *Smådala slope : Evaluation of the stability of a natural slope with a creep model*. BIG (Branschsamverkan i Grunden). Göteborg, Sweden.

Karstunen, M., & Koskinen, M. (2008). Plastic anisotropy of soft reconstituted clays. *Canadian Geotechnical Journal*, *45*(3), 314–328.

Kleman, J., & Hättestrand, C. (1999). Frozen-bed Fennoscandian and Laurentide ice sheets during the last glacial maximum. *Nature*, *402*(6757), 63–66.

Klingberg, F., Påsse, T., & Levander, J. (2006). *Bottenförhållanden och geologisk utveckling i Göta älv*. Sveriges geologiska undersökning.

Koskinen, M., Karstunen, M., & Wheeler, S. J. (2002). Modelling destructuration and anisotropy of a natural soft clay. In P. Mestat (Ed.), *Proceedings of the 5th European Conference on Numerical Methods in Geotechnical Engineering* (pp. 11–20). Presses de l'ENPC, Paris.

Krabbenhoft, K. (2016). *OptumG2: Theory* (K. Krabbenhoft, A. Lymain, & J. Krabbenhoft, Eds.). Optum Computational Engineering.

Krahn, J. (2003). The 2001 R.M. Hardy Lecture: The limits of limit equilibrium analyses. *Canadian Geotechnical Journal*, *40*(3), 643–660.

Lafleur, J., Silvestri, V., Asselin, R., & Soulié, M. (1988). Behaviour of a test excavation in soft Champlain Sea clay. *Canadian Geotechnical Journal*, *25*(4), 705–715.

Lefebvre, G. (1996). Soft sensitive clays. In A. Turner & R. Schuster (Eds.), *Landslides: investigation and mitigation* (Special Re, pp. 607–619). Transportation Research Board, National Academic Press.

Lefebvre, G., & LeBoeuf, D. (1987). Rate effects and cyclic loading of sensitive clays. *Journal of Geotechnical Engineering*, *113*(5), 476–489.

Lehtonen, V. (2011). *Instrumentation and analysis of a railway embankment failure experiment. Research report of the Finnish Transport agency, 29/2011*. Finnish Transport Agency. Helsinki.

Leoni, M., Karstunen, M., & Vermeer, P. A. (2008). Anisotropic creep model for soft soils. *Géotechnique*, *58*(3), 215–226.

Leroueil, S., & Vaughan, P. R. (1990). The general and congruent effects of structure in natural soils and weak rocks. *Géotechnique*, *40*(3), 467–488.

Leroueil, S. (2001). Natural slopes and cuts: Movement and failure mechanisms. *Géotechnique*, *51*(3), 197–243.

Leroueil, S., & Locat, J. (1998). Slope movements — Geotechnical characterization, risk assessment and mitigation. In D. Moore & O. Hungr (Eds.), *Proceedings Eighth International Congress International Association for Engineering Geology and the Environment* (pp. 933–944). A.A. Balkema, Rotterdam, Brookfield.

Leroueil, S., Roy, M., Rochelle, P. L., Brucy, F., & Tavenas, F. A. (1979). Behavior of destructured natural clays. *Journal of the Geotechnical Engineering Division*, *105*(6), 759–778.

Leshchinsky, B. (2013). Comparison of limit equilibrium and limit analysis for complex slopes. *Geo-Congress 2013: Stability and Performance of Slopes and Embankments III*, 1280–1289.

Leshchinsky, B. (2015). Bearing capacity of footings placed adjacent to c'-ϕ' slopes. *Journal of Geotechnical and Geoenvironmental Engineering*, *141*(6).

Leshchinsky, B., & Ambauen, S. (2015). Limit equilibrium and limit analysis: Comparison of benchmark slope stability problems. *Journal of Geotechnical and Geoenvironmental Engineering*, *141*(10), 04015043.

Li, S. Y., Li, D.-D., Liu, H.-D., Wang, S.-W., Geng, Z., & Peng, B. (2021). Formation and failure mechanism of the landslide: a case study for Huaipa, Western Henan, China. *Environmental Earth Sciences*, *80*(15), 1–12.

Li, Y., Zhang, W., & Zhang, R. (2022). Numerical investigation on performance of braced excavation considering soil stress-induced anisotropy. *Acta Geotechnica*, *17*(2), 563–575.

Liang, T., & Knappett, J. A. (2017). Newmark sliding block model for predicting the seismic performance of vegetated slopes. *Soil Dynamics and Earthquake Engineering*, *101*(March 2016), 27–40.

LimitState. (2021). *LimitState:GEO Manual version 3.6.1* (May 2021). LimitState Ltd.

Lucas, D., Herzog, R., Iten, M., Buschor, H., Kieper, A., Askarinejad, A., & Springman, S. M. (2020). Modelling of landslides in a scree slope induced by groundwater and rainfall. *International Journal of Physical Modelling in Geotechnics*, *20*(4), 177–197.

Lundgren, L., & Rapp, A. (1974). A complex landslide with destructive effects on the water supply of Morogoro town, Tanzania. *Geografiska Annaler. Series A, Physical Geography*, *56*(3/4), 251–260.

Morgenstern, N. R., & Price, V. E. (1965). The analysis of the stability of general slip surfaces. *Géotechnique*, *15*(1), 79–93.

Nordman, M., Peltola, A., Bilker-Koivula, M., & Lahtinen, S. (2023). Past and future sea level changes and land uplift in the Baltic Sea seen by geodetic observations. In J. T. Freymueller & L. Sánchez (Eds.), *Beyond 100: The Next Century in Geodesy* (pp. 161–167). Springer International Publishing.

Olsen, L., Sveian, H., Bergstrøm, B., Ottesen, D., & Rise, L. (2013). Quaternary glaciations and their variations in Norway and on the Norwegian continental shelf. In L. Olsen, O. Fredin, & O. Olesen (Eds.), *Quaternary Geology of Norway* (pp. 27–78). Geological Survey of Norway Special Publication.

Perzyna, P. (1963). The constitutive equations for rate sensitive plastic materials. *Quarterly of Applied Mathematics*, *20*(4), 321–332.

Perzyna, P. (1966). Fundamental problems in viscoplasticity. In G. G. Chernyi, H. L. Dryden, P. Germain, L. Howarth, W. Olszak, W. Prager, R. F. Probstein, & H. Ziegler (Eds.), *Advances in Applied Mechanics* (pp. 243–377). Elsevier.

Petterson, K. E. (1916). Kajraset i Göteborg den 5:te mars 1916. *Teknisk Tidskrift*, *V.U.h*(30 and 31), 281–287.

Phoon, K. K., & Kulhawy, F. H. (1999). Characterization of geotechnical variability. *Canadian Geotechnical Journal*, *36*(4), 612–624.

PLAXIS bv. (2021). *PLAXIS CONNECT Edition V21.01 General information manual* (R. Brinkgreve, S. Kumarswamy, W. Swolfs, F. Fonesca, N. Ragi Manoj, I. Zampich, & N. Zalamea, Eds.). Netherlands, Bentley Systems.

Quigley, R. M., & Thompson, C. D. (1966). The fabric of anisotropically consolidated sensitive marine clay. *Canadian Geotechnical Journal*, *3*(2), 61–73.

Rankka, K., Andersson-Sköld, Y., Hultén, C., Larsson, R., Leroux, V., & Dahlin, T. (2004). *Quick clay in Sweden*. Swedish Geotechnical Institute. Linköping.

Roscoe, K. H., & Burland, J. B. (1968). On the generalized stress-strain behavior of "wet" clay. In J. Heyman & F. A. Leckie (Eds.), *Engineering plasticity* (pp. 535–609). Cambridge University Press.

Roscoe, K. H., Schofield, A. N., & Wroth, C. P. (1958). On the yielding of soils. *Géotechnique*, *8*(1), 22–53.

Saito, M. (1965). Forecasting the time of occurrence of a slope failure. *Proceedings of the 6th International Conference in Soil Mechanics and Foundation Engieering th Int. Conf. Soil Mechanics and Foundation Eng*, 537–541.

Sällfors, G. (1975). *Preconsolidation pressure of soft, high-plastic clays* (Doctoral dissertation). Chalmers University of Technology.

Schlögl, M., & Matulla, C. (2018). Potential future exposure of European land transport infrastructure to rainfall-induced landslides throughout the 21st century. *Natural Hazards and Earth System Sciences*, *18*(4), 1121–1132.

Schofield, A. N., & Wroth, P. (1968). *Critical state soil mechanics*. McGraw-Hill.

Sellin, C. (2019). On evaluating slope stability in sensitive clay -a comparison of methods through a case study. In D. Ülgen, A. Saygili, M. R. Kahyaoğlu, S. Durmaz, O. Toygar, & A. Göçügenci (Eds.), *Proceedings of the 27th European Young Geotechnical Engineers Conference* (pp. 249–254). Turkish Society for ISSMGE.

Sellin, C., Abed, A., Dijkstra, J., Karlsson, M., & Smith, C. C. (2023a). Anisotropic strength in discontinuity layout optimisation for undrained slope stability analysis. *Unpublished manuscript*.

Sellin, C., Karlsson, M., & Karstunen, M. (2023b). Impact of rate-dependency on slope stability in sensitive clays. *Manuscript submitted for publication*.

Sellin, C., & Karstunen, M. (2023). Slope stability assessment in sensitive clay with an advanced constitutive model. In L. Zdravković, S. Kontoe, D. Taborda, & A. Tsiampousi (Eds.), *Proceedings of the 10th European Conference on Numerical Methods in Geotechnical Engineering* (pp. 1–6). CRC Press.

SGI. (2012). *Landslide risks in the Göta River valley in a changing climate Final report Part 1 - Societal concequenses*. Swedish Geotechnical Institute. Linköping.

SGI. (2022). *Framtida kostnader till följd av ras, skred och erosion*.

Sheng, D., Sloan, S. W., & Yu, H. S. (2000). Aspects of finite element implementation of critical state models. *Computational Mechanics*, *26*(2), 185–196.

Sivasithamparam, N., Karstunen, M., & Bonnier, P. (2015). Modelling creep behaviour of anisotropic soft soils. *Computers and Geotechnics*, *69*, 46–57.

Skredkommissionen. (1995). *Anvisningar för släntstabilitetsutredningar Rapport 3:95*. Statens Geotekniska Institut. Linköping.

Sloan, S. W. (2013). Geotechnical stability analysis. *Géotechnique*, *63*(7), 531–572.

Smith, C., & Gilbert, M. (2007). Application of discontinuity layout optimization to plane plasticity problems. *Proceedings of the Royal Society A: Mathematical, Physical and Engineering Sciences*, *463*(2086), 2461–2484.

Smith, C. C., & Tatari, A. (2016). Limit analysis of reinforced embankments on soft soil. *Geotextiles and Geomembranes*, *44*(4), 504–514.

Sowers, G. B., & Sowers, G. F. (1951). *Introductory soil mechanics and foundations* (2nd). Macmillan.

Spencer, E. (1967). A method of analysis of the stability of embankments assuming parallel inter-slice forces. *Géotechnique*, *17*(1), 11–26.

Stroeven, A. P., Hättestrand, C., Kleman, J., Heyman, J., Fabel, D., Fredin, O., Goodfellow, B. W., Harbor, J. M., Jansen, J. D., Olsen, L., Caffee, M. W., Fink, D., Lundqvist, J., Rosqvist, G. C., Strömberg, B., & Jansson, K. N. (2016). Deglaciation of Fennoscandia. *Quaternary Science Reviews*, *147*, 91–121.

Swan, C. C., & Seo, Y.-K. (1999). Limit state analysis of earthen slopes using dual continuum/FEM approaches. *International Journal for Numerical and Analytical Methods in Geomechanics*, *23*(12), 1359–1371.

Take, W. A., & Bolton, M. D. (2011). Seasonal ratcheting and softening in clay slopes, leading to first-time failure. *Géotechnique*, *61*(9), 757–769.

Tavenas, F., & Leroueil, S. (1977). Effects of stresses and times on yielding of clays. *Proceedings of the 9th International Conference on Soil Mechanics and Foundation Engineering*, 319–326.

Tavenas, F., Leroueil, S., La Rochelle, P., & Roy, M. (1978). Creep behaviour of an undisturbed lightly overconsolidated clay. *Canadian Geotechnical Journal*, *15*(3), 402–423.

Terzaghi, K. (1950). Mechanism of landslides. *Application of geology to engineering practice* (pp. 83–123). Geological Society of America.

Tornborg, J., Karlsson, M., & Karstunen, M. (2023). Permanent sheet pile wall in soft sensitive clay. *Journal of Geotechnical and Geoenvironmental Engineering*, *149*(6), 05023003.

Tornborg, J., Karlsson, M., Kullingsjö, A., & Karstunen, M. (2021). Modelling the construction and long-term response of Göta Tunnel. *Computers and Geotechnics*, *134*, 104027.

Ukritchon, B., & Boonyatee, T. (2015). Soil parameter optimization of the NGI-ADP constitutive model for Bangkok soft clay. *Geotechnical Engineering of the SEAGS & AGSSEA*, *46*(1), 28–36.

United Nations, D. o. E., & Affairs, S. (2019). *World Urbanization Prospects: The 2018 Revision (ST/ESA/SER.A/420)*. United Nations.

Utili, S., & Crosta, G. B. (2015). Chapter 13 - Analysis tools for mass movement assessment. *Landslide Hazards, Risks, and Disasters* (pp. 441–465). Academic Press.

Vaid, Y. P., Robertson, P. K., & Campanella, K. G. (1979). Strain rate behaviour of Saint-Jean-Vianney clay. *Canadian Geotechnical Journal*, *16*(1), 34–42.

Varnes, D. J. (1958). Slope movement types and processes. In R. Schuster & R. Krizek (Eds.), *Landslides, analysis and control, Special report 176* (pp. 11–33). Transportation research board, National Academy of Sciences.

Vulliet, L., & Hutter, K. (1988). Viscous-type sliding laws for landslides. *Canadian Geotechnical Journal*, *25*(3), 467–477.

Wheeler, S. J., Näätänen, A., Karstunen, M., & Lojander, M. (2003). An anisotropic elastoplastic model for soft clays. *Canadian Geotechnical Journal*, *40*(2), 403–418.

Winkler, K., Fuchs, R., Rounsevell, M., & Herold, M. (2021). Global land use changes are four times greater than previously estimated. *Nature Communications*, *12*(2501), 1–10.

Yin, Z. Y., Chang, C. S., Karstunen, M., & Hicher, P. Y. (2010). An anisotropic elastic-viscoplastic model for soft clays. *International Journal of Solids and Structures*, *47*(5), 665–677.

Yin, Z.-Y., Karstunen, M., Chang, C. S., Koskinen, M., & Lojander, M. (2011). Modeling time-dependent behavior of soft sensitive clay. *Journal of Geotechnical and Geoenvironmental Engineering*, *137*(11), 1103–1113.

Zheng, G., Zhao, J., Zhou, H., & Zhang, T. (2019). Ultimate bearing capacity of strip footings on sand overlying clay under inclined loading. *Computers and Geotechnics*, *106*, 266–273.

Zhou, C., Yin, J.-H., Zhu, J.-G., & Cheng, C.-M. (2005). Elastic anisotropic viscoplastic modeling of the strain-rate-dependent stress – strain behavior of K0-consolidated natural marine clays in triaxial shear tests. *International Journal of Geomechanics*, *5*(3), 218–232.

Zhou, H., Zheng, G., He, X., Xu, X., Zhang, T., & Yang, X. (2018a). Bearing capacity of strip footings on c–ϕ soils with square voids. *Acta Geotechnica*, *13*(3), 747–755.

Zhou, H., Zheng, G., Yin, X., Jia, R., & Yang, X. (2018b). The bearing capacity and failure mechanism of a vertically loaded strip footing placed on the top of slopes. *Computers and Geotechnics*, *94*, 12–21.

Zhu, J. G., Yin, J. H., & Luk, S. T. (1999). Time-dependent stress-strain behavior of soft Hong Kong marine deposits. *Geotechnical Testing Journal*, *22*(2), 118–126.

Zienkiewicz, O. C., Humpheson, C., & Lewis, R. W. (1975). Associated and non-associated visco-plasticity and plasticity in soil mechanics. *Géotechnique*, *25*(4), 671–689.